1 Single-Electron Devices

Jürgen Weis
Max-Planck-Institut für Festkörperforschung, 70569 Stuttgart, Germany

Contents

1.1 Introduction

The electrical charge is quantized in the elementary quantum $-e$ carried by single electrons. In mesoscopic systems at sufficient low temperature, this discrete elementary charge can give rise to peculiar electrostatic effects. With achieving the ability of making small devices on the scale

of less than few hundred nanometers, devices based on single-electron charging effects have been proposed and realized in the last 15 years.

After a brief introduction to the concepts of Coulomb blockade and single-electron charging, some device concepts for applications are presented, but also arrangements for studying basic physics of electrical transport relevant for molecular electronics are discussed. The presented picture for electrical transport through conducting mesoscopic particles ('island') by single-electron tunneling breaks down if correlated electron tunneling takes place. Under certain circumstances, correlated electron tunneling leads even to the conductance of a one-dimensional channel although Coulomb blockade is expected.

For historical reviews, further readings and other approaches to the topic of single-electron devices, the articles [1–8] are recommended. Especially for superconducting devices not treated here, we refer to [9, 10], for proposal of using single-electron devices as qubits to [11] (quantum dots as islands), [12] (superconducting devices).

1.2 Single-Electron Charging Energy and Coulomb Blockade Effect

Fig. 1.1 shows an arrangement of an electrically uncharged *metal island* embedded in a dielectric medium and surrounded by other metal electrodes which are electrically connected. By transfering a single electron from the electrodes to the island, the island is charged negative to $q = -e$ and positive image charges q_1, q_2 spread over the electrodes (see Fig. 1.1b). Note, the overall charge of the system compensates to zero: $-e + q_1 + q_2 = 0$. Similarly, by transfering an electron from the electrically uncharged island to the electrodes, the island is charged positive and negative image charges are induced on the surrounding electrodes (see Fig. 1.1c). The arrangement resembles a capacitor configuration with the capacitance C_Σ where the island reflects one electrode of this capacitor and the others form all together the counter electrode. For both charge configurations ($q = -e$ and $q = e$), the electrostatic energy E_C

$$E_\mathrm{C} = \frac{e^2}{2\,C_\Sigma} \tag{1.1}$$

is stored in the arrangement. The quantity E_C is usually denoted as *single-electron charging energy*[1]. This energy is required for the separation of a single electron from its positive counter charge spread over the other conductors. It is the electrostatic energy barrier felt by the single electron moving onto or from the electrically neutral island.

Usually this energy E_C is not noticeable since the island size and therefore C_Σ is large. However, for $C_\Sigma < 10^{-15}\,\mathrm{F}$ which corresponds[2] to the 'self-capacitance' $C_\Sigma = 4\pi\epsilon_0\epsilon\,R$ of a metallic sphere with radius $R < 1\,\mu\mathrm{m}$ embedded in a dielectric medium with $\epsilon = 10$, E_C exceeds the thermal energy $k_\mathrm{B}T$ at $T = 4$ K. For $C_\Sigma < 3 \cdot 10^{-18}\,\mathrm{F}$ which is fulfilled for $R < 2.8$ nm, even $k_\mathrm{B}T$ at room temperature ($T = 300$ K) is exceeded. From this, we have to conclude that the single-electron charging energy E_C is of importance to describe single-electron movements in systems from mesoscopic size down to atomic size.

[1] Sometimes [2] the quantity e^2/C_Σ is denoted by the same name.

[2] Counter electrode at infinite distance.

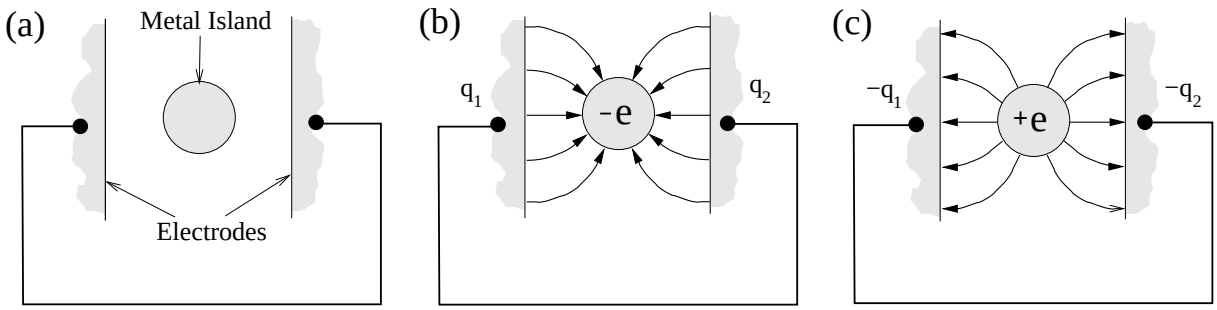

Fig. 1.1: (a) A metal island embedded between electrodes which are electrically connected. Transfering an electron onto the island (b) or taking off the electron from the island (c) charges the capacitor formed by the island and the electrodes.

A simple two-terminal arrangement for discussing the consequence is shown in Fig. 1.2a. A small island is embedded between two lead electrodes denoted as *source* S and *drain* D. Thin insulators separate the island from the two leads. These layers should be thin enough that – due to quantum mechanics – tunneling of electrons through the insulator layers is possible, thick enough that it is plausible to describe single electrons in the system as being localized either on the metal island or the lead electrodes. Since the metal island is *almost isolated*, the total charge on the metal electrodes is considered as being quantized in the elementary charge e. Due to E_{C} which is required for recharging the island by a single electron entering or leaving, electrical transport is suppressed around $V_{\mathrm{DS}} = 0$ if $E_{\mathrm{C}} \gg k_{\mathrm{B}}T$ (*Coulomb blockade effect* of electrical transport).

With increasing the bias voltage $V_{\mathrm{DS}} > 0$, the electrostatic energy barriers for adding an electron from source

$$\Delta E_{\mathrm{S}\to\mathrm{I}} = E_{\mathrm{C}} - e\,\frac{C_{\mathrm{D}}}{C_{\Sigma}}\,V_{\mathrm{DS}} \tag{1.2}$$

and the electrostatic energy barrier for an electron leaving to drain

$$\Delta E_{\mathrm{I}\to\mathrm{D}} = E_{\mathrm{C}} + e\,\frac{C_{\mathrm{D}}}{C_{\Sigma}}\,V_{\mathrm{DS}} - e\,V_{\mathrm{DS}} \tag{1.3}$$

are reduced as a consequence of the applied voltage V_{DS} (The respective capacitance circuit is given in Fig. 1.2b). Similar happens for $V_{\mathrm{DS}} < 0$. The suppression of current is finally overcome for

$$|V_{\mathrm{DS}}| \geq V_{\mathrm{DS}}^{(\mathrm{th})} \equiv \min\left(\frac{e}{2\,C_{\mathrm{S}}}; \frac{e}{2\,C_{\mathrm{D}}}\right), \tag{1.4}$$

and the drain-source current $|I_{\mathrm{DS}}|$ rises rapidly with increasing $|V_{\mathrm{DS}}|$. If $E_{\mathrm{C}} \gg k_{\mathrm{B}}T$, for such a two-terminal device a non-linear current-voltage characteristic with threshold values lying symmetrically around $V_{\mathrm{DS}} = 0$ is obtained.

1.3 Concept of a Single-Electron Transistor (SET)

Instead of overcoming the Coulomb blockade by increasing V_{DS}, a *gate electrode* G with variable gate-voltage V_{GS} can be added to the arrangement (see Fig. 1.3a). With increasing gate voltage

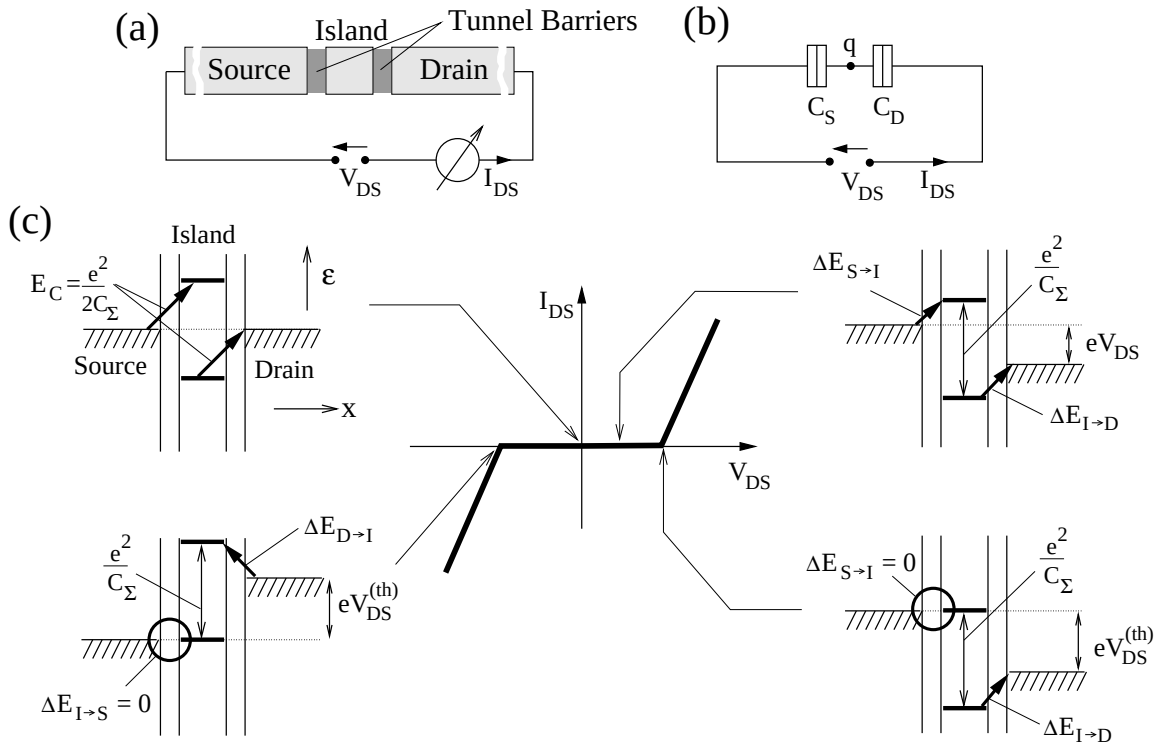

Fig. 1.2: (a) Two-terminal arrangement for discussing the Coulomb blockade effect in electrical transport. (b) The respective capacitance circuit. Note $C_\Sigma = C_\mathrm{S} + C_\mathrm{D}$. (c) Sketch of the expected non-linear $I_\mathrm{DS}(V_\mathrm{DS})$ characteristic with energy schemes for distinct V_DS values reflecting the energetical position of the Fermi levels of the island for charge states $q = -e$ and $q = e$ relatively to the Fermi level of source and drain.

V_GS, the electrostatic potential of the island is shifted due to the capacitance circuit sketched in Fig. 1.3b. With positive going V_GS, negative charge is accumulated on the island – not in a continuous but in a step-like manner as sketched in Fig. 1.3c (*single-electron charging*). The first electron is charged at $V_\mathrm{GS} = V_\mathrm{GS}^{(\mathrm{th})}$ when the electrostatic energy for an electron on the island is lowered just compensating for E_C, i.e.,

$$\Delta E_{\mathrm{S}\to\mathrm{I}} = E_\mathrm{C} - e\,\frac{C_\mathrm{G}}{C_\Sigma}\,V_\mathrm{GS} \stackrel{!}{=} 0\;, \tag{1.5}$$

leading to the threshold voltage

$$V_\mathrm{GS}^{(\mathrm{th})} = \frac{E_\mathrm{C}}{e\,C_\mathrm{G}/C_\Sigma} = \frac{e}{2\,C_\mathrm{G}}\;. \tag{1.6}$$

At this gate-voltage value, the charge state of the island fluctuates by e. Applying a small drain-source voltage V_DS, a directed current is measured between source and drain – carried by single electrons passing one after the other the island.

What about charging the electrically neutral island by ΔN electrons from the source lead? The electrostatic energy stored in such a charge configuration ($q = -\Delta N\,e$) – under the condition that V_DS and V_GS are fixed – is given by

$$E_\mathrm{elst}(\Delta N; V_\mathrm{GS}, V_\mathrm{DS}) = -\Delta N\,e\left(\frac{C_\mathrm{G}}{C_\Sigma}\,V_\mathrm{GS} + \frac{C_\mathrm{D}}{C_\Sigma}\,V_\mathrm{DS}\right) + \frac{(\Delta N\,e)^2}{2\,C_\Sigma}\;. \tag{1.7}$$

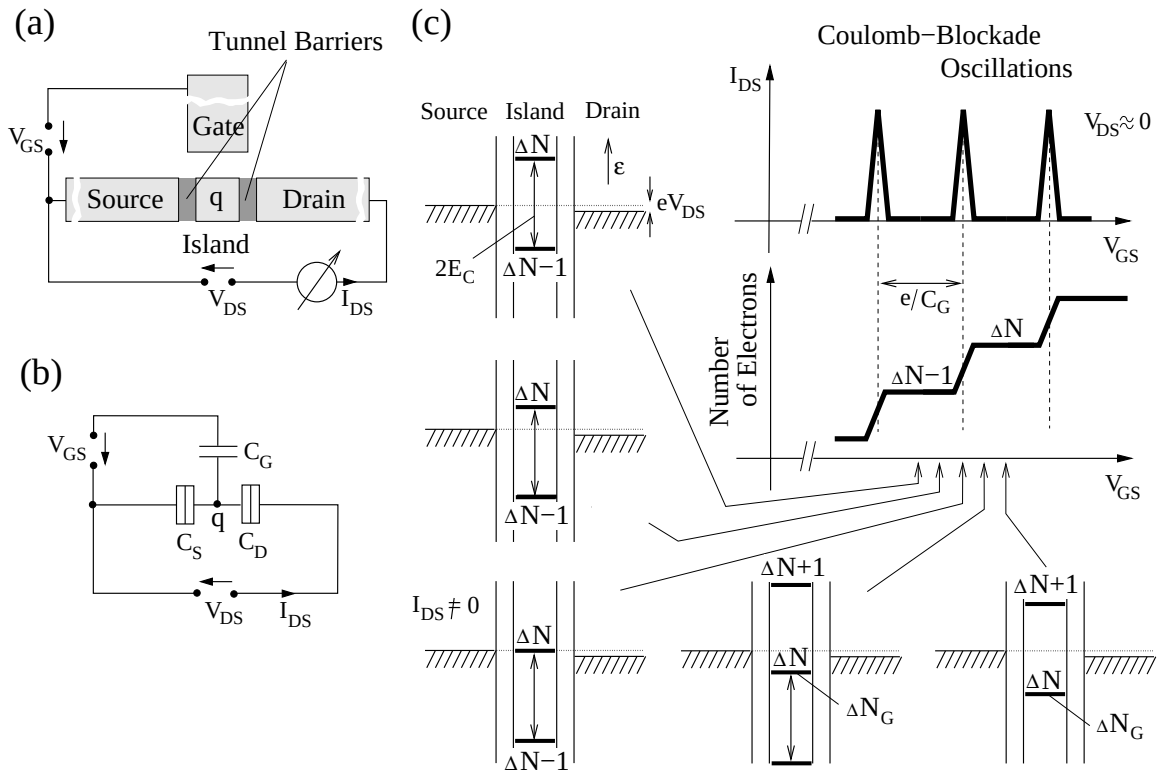

Fig. 1.3: (a) Three-terminal arrangement of a single-electron transistor. (b) The respective capacitance circuit. Note $C_\Sigma = C_S + C_D + C_G$. (c) With increasing gate voltage V_{GS}, electrons are accumulated on the island. Whenever the charge state can energetically fluctuate by e, i.e., the energy for two charge states is degenerate, current I_{DS} flows for small applied V_{DS} through the island, leading to a periodically modulated $I_{DS}(V_{GS})$-characteristic – the Coulomb blockade oscillations. For distinct V_{GS} values, the respective energy schemes are given.

The first term describes the potential energy of ΔN electrons at the electrostatic potential which is found due to the capacitance divider at the electrically neutral island. The second term takes into account the work which has to be done to separate the charge $q = -\Delta N\, e$ from its counter charge spread over the electrodes source S, drain D and gate G.

Having already charged the island with ΔN electrons, the next electron '$\Delta N + 1$' moving from source to the charged island feels at fixed applied V_{GS} and V_{DS} the electrostatic energy difference

$$\begin{aligned} \Delta E_{S\to I}(\Delta N+1; V_{GS}, V_{DS}) &= E_{elst}(\Delta N+1; V_{GS}, V_{DS}) - E_{elst}(\Delta N; V_{GS}, V_{DS}) \\ &= \left(\Delta N + \tfrac{1}{2}\right) \frac{e^2}{C_\Sigma} - e\,\frac{C_G}{C_\Sigma}\, V_{GS} - e\,\frac{C_D}{C_\Sigma}\, V_{DS}\ . \end{aligned} \tag{1.8}$$

Similarly, having ΔN electrons on the island, the electron 'ΔN' feels for moving towards drain the electrostatic energy difference

$$\begin{aligned} \Delta E_{I\to D}(\Delta N; V_{GS}, V_{DS}) &= E_{elst}(\Delta N-1; V_{GS}, V_{DS}) - e\,V_{DS} - E_{elst}(\Delta N; V_{GS}, V_{DS}) \\ &= -\left(\Delta N - \tfrac{1}{2}\right) \frac{e^2}{C_\Sigma} + e\,\frac{C_G}{C_\Sigma}\, V_{GS} - e\left(1 - \frac{C_D}{C_\Sigma}\right) V_{DS}\ . \end{aligned} \tag{1.9}$$

It contains the final electrostatic energy $-e\,V_{DS}$ of the electron on the drain site.

The energy differences $E_{elst}(\Delta n; V_{GS}, V_{DS}) - E_{elst}(\Delta n-1; V_{GS}, V_{DS})$ with $n \in \{\cdots, N-1, N, N+$

$1, \cdots\}$ define an energy ladder with fixed energy level spacing $2\,E_\mathrm{C} = e^2/C_\Sigma$ which shifts linearly with V_DS and V_GS: For given V_DS and V_GS the level 'Δn' reflects the energetical position of the Fermi level on the island relatively to the Fermi levels of the two leads if the island is charged to $q = -\Delta n\, e$. The relative position of this energy ladder are given for distinct parameters $(V_\mathrm{GS}; V_\mathrm{DS} \approx 0)$ in the energy schemes of Fig. 1.3c. In thermodynamic equilibrium, $\Delta n = \Delta N_\mathrm{G}$ additional electrons are trapped on the island if

$$\text{for } V_\mathrm{DS} \geq 0 \qquad \Delta E_{\mathrm{S}\to\mathrm{I}}(\Delta N_\mathrm{G}+1; V_\mathrm{GS}, V_\mathrm{DS}) > 0 \text{ and } \Delta E_{\mathrm{I}\to\mathrm{D}}(\Delta N_\mathrm{G}; V_\mathrm{GS}, V_\mathrm{DS}) > 0\,, \quad (1.10)$$

$$\text{for } V_\mathrm{DS} \leq 0 \qquad \Delta E_{\mathrm{I}\to\mathrm{S}}(\Delta N_\mathrm{G}; V_\mathrm{GS}, V_\mathrm{DS}) > 0 \text{ and } \Delta E_{\mathrm{D}\to\mathrm{I}}(\Delta N_\mathrm{G}+1; V_\mathrm{GS}, V_\mathrm{DS}) > 0\,. \quad (1.11)$$

Whenever $\Delta E_{\mathrm{S}\to\mathrm{I}} = 0$ or $\Delta E_{\mathrm{I}\to\mathrm{D}} = 0$, the charge state of the island can fluctuate by e. Applying a small drain-source voltage V_DS, a directed current is measured between source and drain. With changing the gate voltage V_GS at small V_DS, the current is modulated with the gate voltage period

$$\Delta V_\mathrm{GS} = \frac{e}{C_\mathrm{G}} \quad (1.12)$$

as sketched in Fig. 1.3c. This characteristic is denoted as *Coulomb blockade oscillations* (CBOs). Since the current is carried by single electrons passing the island one-by-one, the three-terminal device with such a characteristic is named *single-electron transistor* (SET) [13, 14].

Evaluating (1.10) and (1.11) allows to define transport regions for a single-electron transistor as a function of the drain-source voltage V_DS and the gate voltage V_GS. The result is sketched in Fig. 1.4: Light grey shaded are the *regions of Coulomb blockade* (fulfilling (1.10) and (1.11)) at low temperature where the electron number is fixed. Fluctuations by only one electron charge $-e$ are possible in the adjacent regions. These are the *regions of single-electron tunneling* since there the electrons are passing the island one after the other. Along the gate voltage axis with $V_\mathrm{DS} \approx 0$, the Coulomb blockade oscillations are obtained. With further increasing $|V_\mathrm{DS}|$, more and more charge configurations become energetically possible. For distinct parameter configurations $(V_\mathrm{DS}, V_\mathrm{GS})$, the respective energy scheme are depicted. For the metal single-electron transistor, the transport characteristics are periodic in V_GS: With each gate voltage change $\Delta V_\mathrm{GS} = e/C_\mathrm{G}$, the same electrostatic energy barriers for recharging the island are present – only with one electron more trapped on the island.

The borderlines between Coloumb blockade and single-electron tunneling regime have the slopes

$$\left.\frac{\mathrm{d}V_\mathrm{GS}}{\mathrm{d}V_\mathrm{DS}}\right|_{\Delta E_{\mathrm{S}\to\mathrm{I}}=0} = -\frac{C_\mathrm{D}}{C_\mathrm{G}} \qquad \text{and} \qquad \left.\frac{\mathrm{d}V_\mathrm{GS}}{\mathrm{d}V_\mathrm{DS}}\right|_{\Delta E_{\mathrm{I}\to\mathrm{D}}=0} = \frac{C_\Sigma - C_\mathrm{D}}{C_\mathrm{G}}\,. \quad (1.13)$$

Note, these relations are valid for the special choice of the source electrode as the reference electrode for all applied voltages.

One should also realize that the notation of the two different transport regions of a single-electron transistor – Coulomb blockade and single-electron tunneling regime – as a function of V_DS and V_GS are obtained due to energy considerations. Multi-electron transport is predicted at higher $|V_\mathrm{DS}|$ values where regions of more than two charge states could coexist. However, SETs with strongly asymmetric tunnel barriers also show single-electron transport at these higher $|V_\mathrm{DS}|$ values: An electron leaving via the thicker tunnel barrier is almost immediately replaced by an electron tunneling through the thinner tunnel barrier; for opposite drain-source

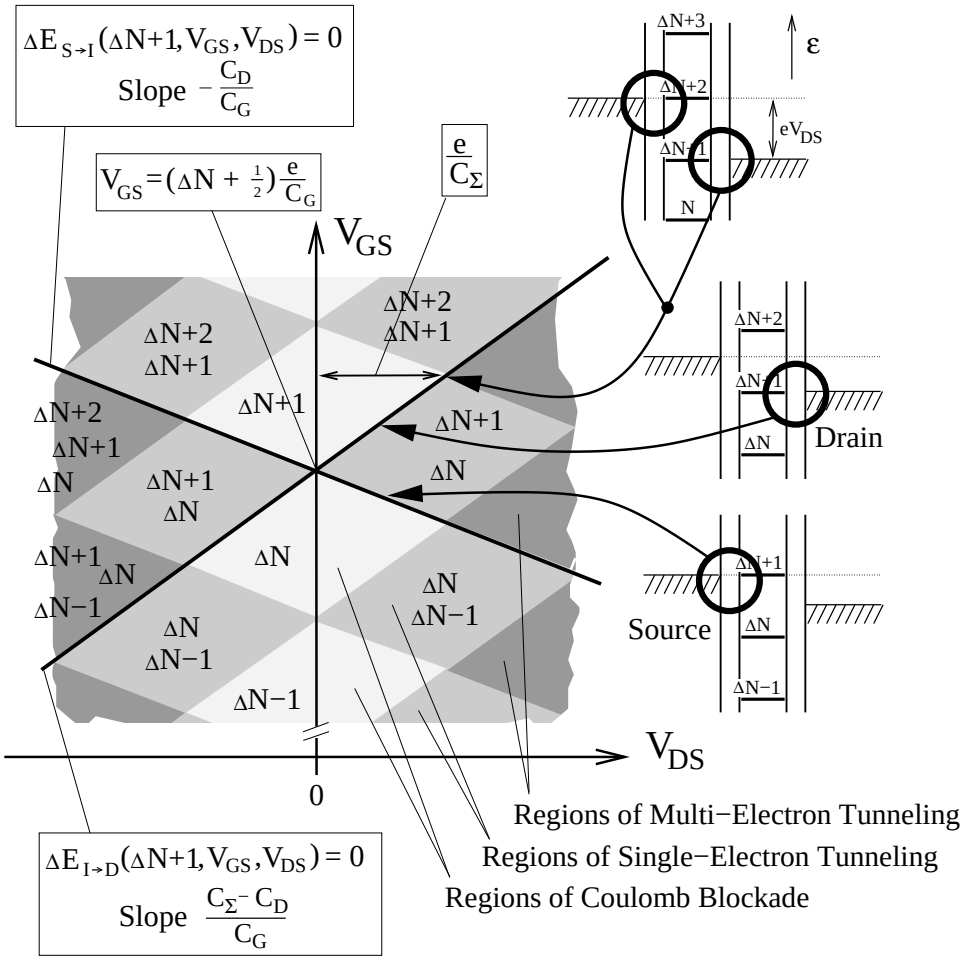

Fig. 1.4: Transport regions of a single-electron transistor as a function of V_{DS} and V_{GS}. This pattern is usually referred to as 'diamond-like'.

voltage an electron entering the island via the thicker tunnel barrier leaves usually faster via the thinner barrier than another electron can enter via the thicker barrier. The dynamics of the system restrict the charge fluctuations on the island to e. Under such conditions the current I_{DS} increases in a step-like manner with increasing $|V_{\mathrm{DS}}|$ whenever another charge state has become energetically available, i.e., a boundary line in Fig. 1.4 is crossed with increasing $|V_{\mathrm{DS}}|$. The so-called *Coulomb-staircase* characteristic in $I_{\mathrm{DS}}(V_{\mathrm{DS}})$ is obtained [15].

1.4 Examples for the Realization of Single-Electron Transistors

Two examples for the realization of a single-electron transistor are discussed in this section. First, a device made from metal is shown to demonstrate that small metal islands indeed offer transport characteristics dominated by Coulomb blockade and single-electron charging effects although more than 10^9 electrons are actually present in the condcution band of the island. In contrast, as the second realization, a SET made from a semiconductor material is presented. It contains a *quantum dot* as the island with a small number of trapped electrons (about 10 to 20) and a discrete excitation spectrum, and even allows the in-situ control over the tunnel coupling between island and leads. Due to their *in-situ tunability*, such quantum dot systems can act as

model systems for studying basic phenomena in electrical transport through single molecules or atoms embedded between lead electrodes.

Other arrangements and realizations of single-electron transistors are presented within this school (for instance, vertical quantum dot devices by K.M. Indlekofer).

1.4.1 Single-Electron Transistor Made from Metal

An example for a metal single-electron transistor made from aluminum is shown in 'Cross Section 1' of Fig. 1.5a and as a scanning-electron microscope image in Fig. 1.5b. The devices is fabricated by using a two-angle evaporation technique also used to fabricate the first SET [16]: With electron-beam lithography, a two-layer organic resist is patterned resulting in openings to the substrate with large undercut (see 'Cross Section 2'). In vacuum, aluminum layers are evaporated

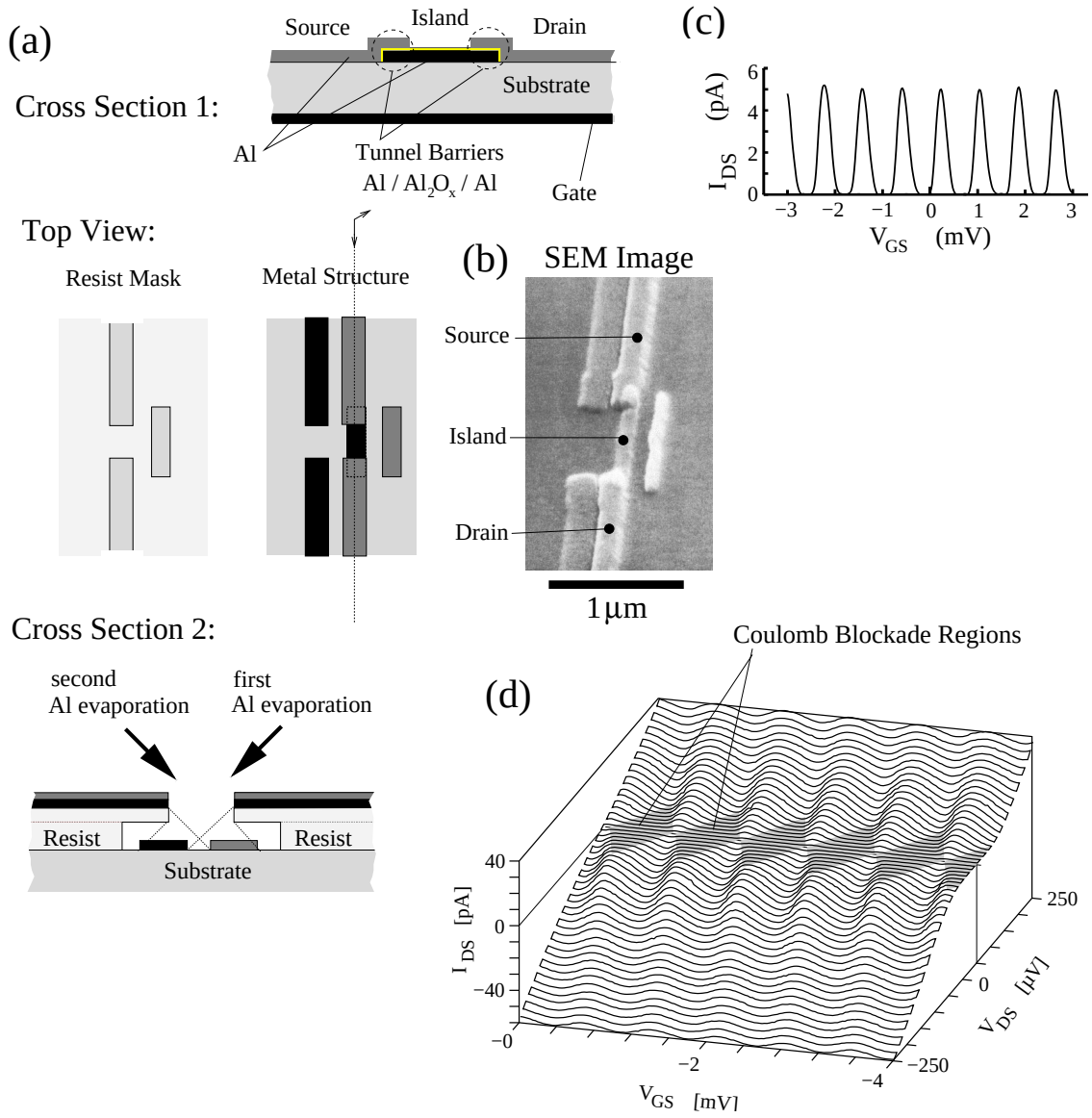

Fig. 1.5: SET made from metal: (a) Fabrication process (see text). (b) Scanning electron microscope image. (c) Coulomb-blockade oscillations. (d) $I_{\mathrm{DS}}(V_{\mathrm{DS}}, V_{\mathrm{GS}})$ characteristics measured at $T = 0.1\,\mathrm{K}$. (from Y.Y. Wei, J. Hüls et al., MPI-FKF)

twice under different angles through the openings onto the substrate. By an in-situ oxidation *between* first and second evaporation process, a thin aluminum oxide of few nanometers is formed on the first aluminum layer. The resist is lifted off and a metal structure remains on the substrate. Due to the two different evaporation angles, the metal patterns of the first and second evaporation process are slightly shifted against each other leading to an overlap in certain regions. In the overlap regions, the thin aluminum oxide acts as tunnel barriers between both aluminum layers, whereas the uncovered aluminum is unavoidable oxidized further in air. The island has a length of $1\,\mu$m and a width of $0.1\,\mu$m. The overlap region defining the tunnel barriers towards the leads are $0.1\,\mu$m by $0.1\,\mu$m in size. Coulomb blockade oscillations measured on this device at $T = 0.1\,\mathrm{K}$ for $V_{\mathrm{DS}} = 80\,\mu\mathrm{V}$ are shown in Fig. 1.5c. As the gate electrode, a conductive layer in the substrate 86 nm below the surface is used. Due to the small size of the device, the total capacitance C_Σ – dominated by the overlap regions of the tunnel junctions – is small leading to $E_{\mathrm{C}} \approx 0.1\,\mathrm{meV}$. In Fig. 1.5d the measured $I_{\mathrm{DS}}(V_{\mathrm{DS}}, V_{\mathrm{GS}})$ characteristics of a similar metal single-electron transistor (E_{C} slightly smaller) are shown. Clearly the Coulomb blockade regions are visible. Beyond the respective threshold in V_{DS}, the current I_{DS} increases.

1.4.2 Single-Electron Transistor Containing a Quantum Dot as Island

Quantum dots or *zero-dimensional electron systems* are objects where electrons are confined in a small enclosure allowing the single electron only certain eigenvalues for its energy due to the wave character of electrons as quantum mechanical particles. As sketched in Fig. 1.6, with decreasing the size of the island, the quasi-continuous single-particle energy spectrum (like that of a metal) turns into a discrete one (like that of an atom) if the deBroglie wavelength $\lambda_{\mathrm{F}} = h/\sqrt{2m\,\varepsilon_{\mathrm{F}}}$ of an electron at the Fermi energy ε_{F} of the respective bulk material becomes comparable to the island diameter D.

A realization of a single-electron transistor with a quantum dot as island is shown in Fig. 1.7 – denoted as *split-gate quantum dot system*: Base is a GaAs/$Al_{0.33}Ga_{0.67}$As heterostructure containing a *two-dimensional electron system* at the GaAs/AlGaAs heterojunction interface 86

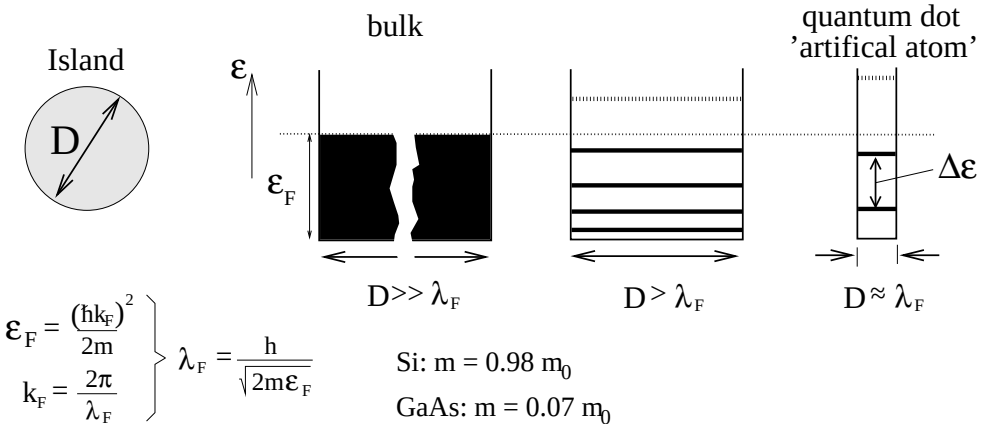

Fig. 1.6: Enclosing electrons to a smaller space, only certain eigenvalues for their kinetic energy become possible (Sketch!). Spatial enclosures with a discrete single-particle spectrum are denoted as quantum dots.

nm below the surface. In GaAs, the effective mass of an electron in the conduction band is rather small, $m = 0.07\,m_0$ where m_0 is the free electron mass. Therefore, single-particle energy level spacing $\Delta\varepsilon$ of several meV are achieved for GaAs islands of few tens of nanometers – large enough to be resolved at low temperature ($k_\mathrm{B}T = 1$ meV at $T = 12$ K). To define the quantum dot system, metallic gates were deposited on top of a mesa remained after partially etching the surface of the heterostructure. The 2DES is electrically contacted by alloying metal at certain regions of the mesa. The diameter of the area between the tips of the gate fingers is about 0.35 μm. With applying negative voltages to the gate electrodes, the 2DES is divided in parts, defining the quantum dot of about 0.2 μm in diameter between the gate fingers, coupled by tunnel barriers to parts of the 2DES acting as source and drain leads. In addition to these topgates, a metallic backgate electrode on the reverse side of the undoped substrate (0.5 mm thick) is used to change the electrostatic potential of the quantum dot by changing the applied voltage V_BS. In Fig. 1.7b, a typical curve of the conductance $I_\mathrm{DS}/V_\mathrm{DS}$ versus the backgate voltage for small drain-source voltage ($V_\mathrm{DS} \approx 5\,\mu$V) is shown – the Coulomb blockade oscillations ($T = 0.1$ K). In contrast to the CBO characteristic shown for the metal single-electron transistor, the peak heights are strongly modulated and the peak distances are not exactly periodic. Both effects are even emphasized by applying a magnetic field as shown in Fig. 1.7c. This indicates that the character of the electronic states of the quantum dot – changed by the magnetic field – affects the electrical transport.

1.5 Quantum Dot as an Interacting N-Electron System: an Artifical Atom with Tunable Properties

Obviously the electrostatic model is not sufficient, i.e., the description has to be extended. A better approach is to ask which is the energy necessary for adding an electron into a given confining potential (defined by gate electrodes with electrostatic potentials $\{V_i\}$, material composition and fixed charges due to donors and acceptors) when already the number N of electrons is present. To answer this, N and $N+1$ electrons have to be treated quantum-mechanically as interacting N and $N+1$ electron systems in the confining potential. A Hamiltonian $\hat{H}(n;\{V_i\})$ of n electrons modeling the electrostatics of realistic quantum dots has the form [17]

$$\hat{H}(n;\{V_i\}) = \sum_{s=1}^{n} \frac{\hat{p}_s^2}{2\,m} - \sum_{s=1}^{n} e\,\Phi_\mathrm{ext}(\hat{r}_s;\{V_i\}) + \tfrac{1}{2}\sum_{s=1}^{n}\sum_{\substack{s'=1\\ s'\neq s}}^{n} e^2\,G(\hat{r}_s,\hat{r}_{s'}) \tag{1.14}$$

where $\hat{p}_s$ and $\hat{r}_s$ denote the momentum and position operator for electron s, respectively. The quantity $G(\vec{r},\vec{r}\,')$ is the electrostatic Green's function for describing the electrostatics of the system without the presence of the n electrons [17]. The physical meaning of $q\,G(\vec{r},\vec{r}\,')$ is the electrostatic potential contribution at position $\vec{r}$ caused by a point charge q located at $\vec{r}\,'$ in the given arrangement. In particular, it describes the electrostatic electron-electron interaction in the quantum dot taking into account the electrostatic screening effect by the electrodes and the dielectric medium. Comparing (1.14) with (1.7), it becomes clear that the effective interaction (last term in (1.14)) is responsible for the Coulomb blockade effect in quantum dots. The confining potential $\Phi_\mathrm{ext}(\vec{r};\{V_i\})$ is given by the fixed charge distribution, the arrangement of the

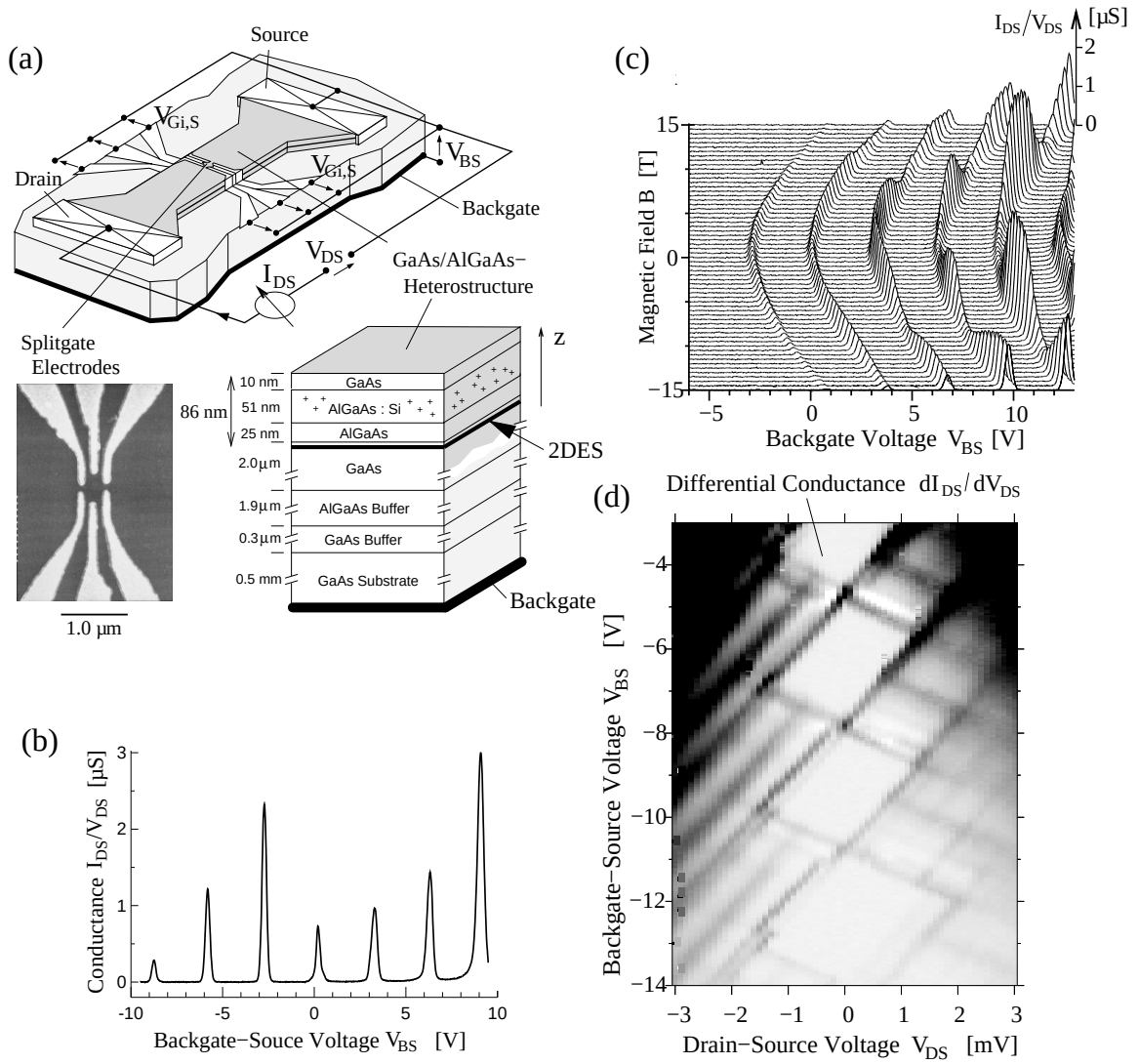

Fig. 1.7: SET with quantum dot as island: (a) Metallic gates on top of a GaAs-AlGaAs heterostructure are used to define a quantum dot system by partially electrostatically depleting a two-dimensional electron system (2DES). (b) Coulomb blockade oscillations as a function of the backgate voltage $V_{\rm BS}$. (c) Coulomb blockade oscillations $I_{\rm DS}(V_{\rm BS})$ for different magnetic fields applied in parallel to the plane of the 2DES. (d) Differential conductance $\mathrm{d}I_{\rm DS}/\mathrm{d}V_{\rm DS}$ in greyscale as a function of $V_{\rm DS}$ and $V_{\rm GS}$. (from J. Weis et al., MPI-FKF)

electrodes and conduction band offsets due to the use of different materials (see Fig. 1.8a). It is *independent* of the electron number confined in the quantum dot. The electrostatic contributions to $\Phi_{\rm ext}(\vec{r};\{V_i\})$ can all be expressed by $G(\vec{r},\vec{r}\,')$ [17]. One should note that the confining potential depends linearly on the electrostatic potentials $\{V_i\}$ of the electrodes, i.e., the electrostatic potential at position $\vec{r}$ is linearly shifted with changing V_i, i.e.,

$$\Phi_{\rm ext}(\vec{r};\{V_i\}) \propto \sum_i \alpha_i(\vec{r})\, V_i \tag{1.15}$$

where the quantity $\alpha_i(\vec{r})$ reflects the fraction of image charge induced by a point charge at position $\vec{r}$ in the arrangment on electrode i.

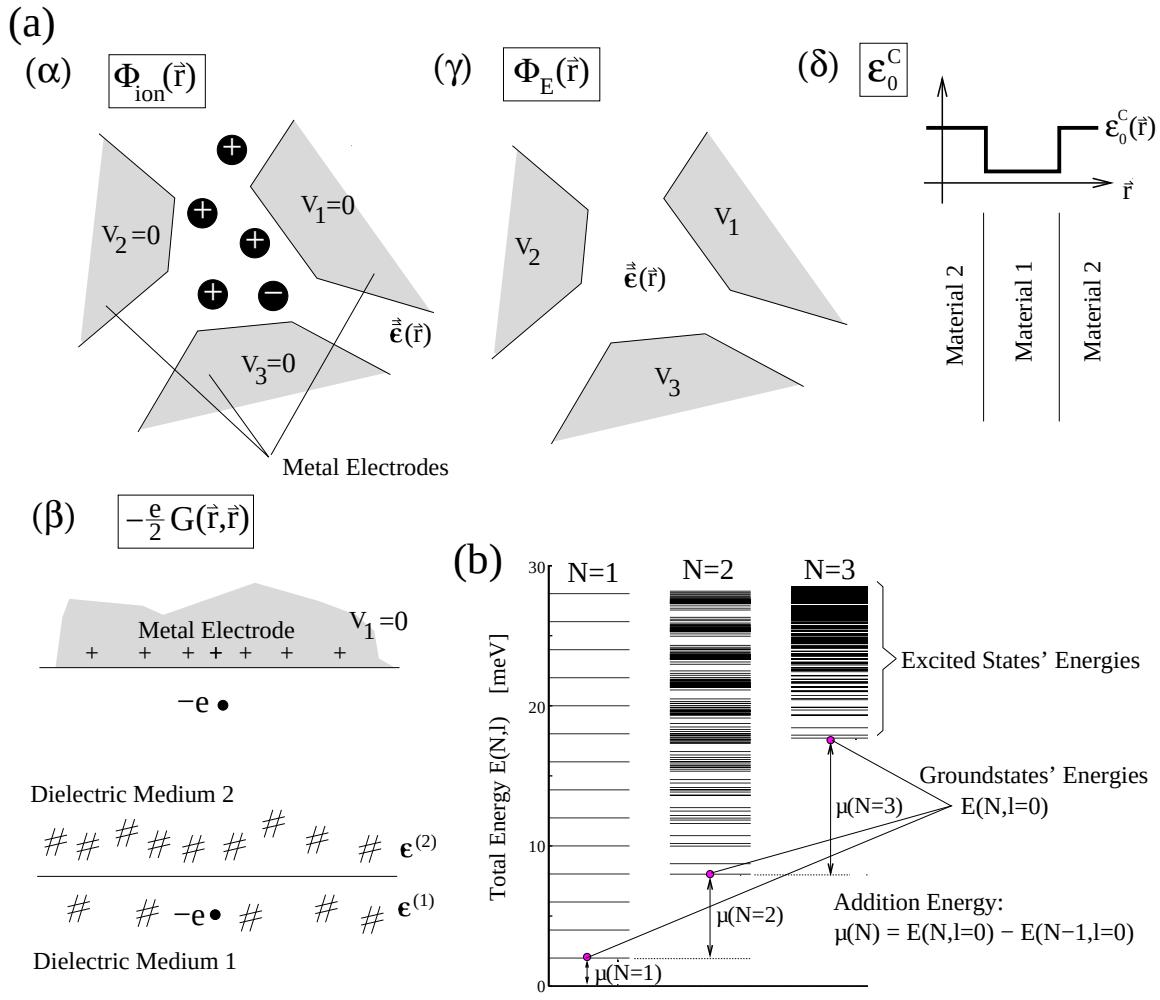

Fig. 1.8: (a) Ingredients defining the confining potential for the electrons: (α) Fixed charge distribution with its image charges induced on the electrodes. (β) Own image charges induced on the electrodes or dielectric interfaces. (γ) Voltages applied to the electrodes. (δ) Conduction band offsets by using different materials. (b) Total energy spectra for one, two and three electrons confined in a parabolic confining potential ($\hbar\omega_0 = 2$ meV) (adopted from D. Pfannkuche et al. [18]).

By solving the Schrödinger equation

$$\hat{H}(n;\{V_i\})\,|n,l;\{V_i\}\rangle = E(n,l;\{V_i\})\,|n,l;\{V_i\}\rangle \tag{1.16}$$

a total energy spectrum $E(n,l;\{V_i\})$ for the confined n-electron system is obtained for a certain set of applied voltages $\{V_i\}$. For convenience, the index l represents a set of quantum numbers that characterizes the different n-electron states $|n,l;\{V_i\}\rangle$ starting from $l = 0$ for the groundstate, and numbering the excited states unambiguously further with increasing energy $E(n,l;\{V_i\})$.

Looking at the Hamiltonian (1.14), it becomes clear why quantum dots have sometimes been denoted as *artifical atoms* [19, 20] with tunable properties: The confining potential for electrons in an atom (the Coulomb potential of the bare nucleus) is replaced by $\Phi_{\rm ext}(\vec{r};\{V_i\})$. The pure Coulomb interaction between electrons in atoms has to be replaced by $e^2\,G(\vec{r},\vec{r}\,')$ if electrostatic

screening due to the dielectric medium or surrounding electrodes is present. In principle, both $\Phi_{\rm ext}(\vec{r};\{V_i\})$ and $G(\vec{r},\vec{r}\,')$ can be designed to purpose.

In a very popular model – the Constant Interaction Model (CIM) [15, 21] – the total energy $E(n;\{V_i\})$ is written as

$$E(n;\{V_i\}) = \sum_{s=1}^{n} \varepsilon_s - n\,e \sum_i \frac{C_i}{C_\Sigma}\,V_i + \frac{(n\,e)^2}{2\,C_\Sigma} - n\,e\cdot\text{const} \tag{1.17}$$

where ε_s is the eigenenergy of the single electron 's' in the (effective) confining potential of the quantum dot. Due to Pauli's principle, single-particle states are sequentially occupied with increasing electron number n and the electron-electron interaction is treated by the constant C_Σ. This description is not generally valid: One should note that – different to atoms – in quantum dots usually the electron-electron interaction is dominating the electronic properties and not the quantization effect on the kinetic energy due to the confining of the electrons. The total energy spectrum becomes complex as shown as an example in Fig. 1.8b. The electrons in the quantum dot feel each other and behave correlated (which is an exciting subject on its own (see for recent review [22])).

1.6 Transport Spectroscopy on Quantum Dot Systems

Having N electrons confined, they will end up in the groundstate $|N,0;\{V_i\}\rangle$ at low temperature. The minimum in energy required for adding another electron to the system is achieved when ending in the groundstate $|N+1,0;\{V_i\}\rangle$ of the $N+1$ electron system. The energy ladder

$$\mu(n;\{V_i\}) \equiv E(n,0;\{V_i\}) - E(n-1,0;\{V_i\})\ ,\ n\in\{\cdots,N-1,N,N+1,\cdots\} \tag{1.18}$$

gives for fixed potentials $\{V_i\}$ by its position relatively to the electrochemical potentials (Fermi levels) $\mu_{\rm S}$ and $\mu_{\rm D}$ of source and drain the energy barriers for recharging the quantum dot by a single electron. Under circumstances this energy ladder is *linearly* shifted with changing one of the applied voltages $V_{\rm GS}$ and $V_{\rm DS}$: The characteristic 'diamond-like' transport regions of a single-electron transistor as shown in Fig. 1.4 are recovered – although not that regular in size. The boundaries between the different charge states in the $V_{\rm DS}$ vs. $V_{\rm GS}$ are obtained with $\mu_{\rm S}-\mu_{\rm D} = e\,V_{\rm DS}$ from

$$\mu(n;\{V_i\}) = \mu_{\rm S} \quad\text{and}\quad \mu(n;\{V_i\}) = \mu_{\rm D} \quad\text{with}\quad n\in\{\cdots,N-1,N,N+1,\cdots\}\ . \tag{1.19}$$

In Fig. 1.7d, the differential conductance $\mathrm{d}I_{\rm DS}/\mathrm{d}V_{\rm DS}$ of the quantum dot system is shown measured as a function of $V_{\rm DS}$ and $V_{\rm BS}$. In the linear greyscale plot, white regions correspond to $\mathrm{d}I_{\rm DS}/\mathrm{d}V_{\rm DS} < -0.1\,\mu$S and black ones to $\mathrm{d}I_{\rm DS}/\mathrm{d}V_{\rm DS} > 2\,\mu$S. Positive peaks in the differential conductance indicate a step-like increase in the current $I_{\rm DS}$ with increasing $|V_{\rm DS}|$, negative ones a step-like decrease. Clearly the Coulomb-blockade regions are identified. In the adjacent single-electron tunneling regions, additional peaks in the differential conductance are observed indicating the opening of other transport channels although the charge state of the quantum dot can only fluctuate by one elementary charge. These can be attributed to electrical transport using in competition excited states of the quantum dot system [23–26].

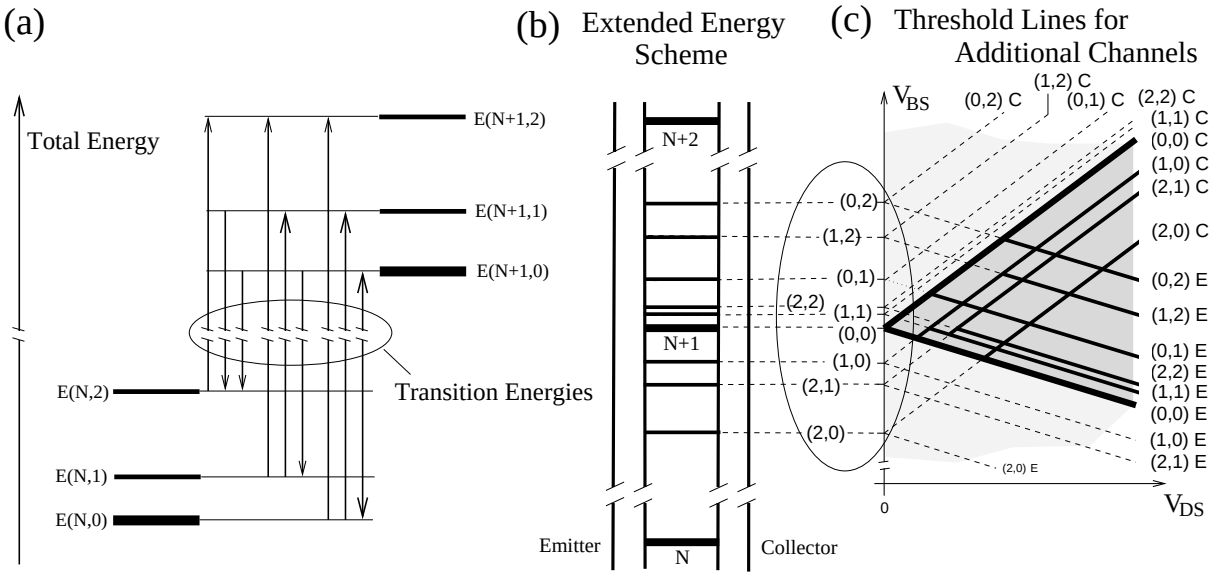

Fig. 1.9: (a) Fictitious total energy spectra of N and $N+1$ electrons confined in the quantum dot. Bold are the groundstate energies. (b) Plot of the transition energies $E(n,k;\{V_i\}) - E(n-1,l;\{V_i\})$ as energy levels. Energy levels representing differences between groundstate energies are bold and marked the respective $n \in \{\cdots, N-1, N, N+1, \cdots\}$. (b) Threshold lines for additional channels extracted from (a). Whether all are visible depends in detail on (quasi-)selection rules and the dynamic of the system.

What is the link between the total energy spectra of n and $n+1$ electron systems and that what is seen in the single-electron tunneling regime ('transport spectrum')? In Fig. 1.9a, the fictitious total energy spectra for N and $N+1$ electrons are given which lead to the energy ladder defined by the transistion energies $E(N+1,k;\{V_i\}) - E(N,l;\{V_i\})$ and plotted in Fig. 1.9b. It includes the transition energy $\mu(N;\{V_i\}) = E(N+1,0;\{V_i\}) - E(N,0;\{V_i\})$ between the groundstates. With changing a gate voltage $V_{\rm GS}$ or the drain-source voltage $V_{\rm DS}$, the energy ladder is shifted, i.e., these levels come in resonance with $\mu_{\rm S}$ or $\mu_{\rm D}$ for certain $(V_{\rm GS}, V_{\rm DS})$ values,

$$E(N+1,k;\{V_i\}) - E(N,l;\{V_i\}) = \mu_{\rm S} \quad \text{or} \quad E(N+1,k';\{V_i\}) - E(N,l';\{V_i\}) = \mu_{\rm D} \tag{1.20}$$

By this, an additional transport channel might be opened on source or drain side, respectively. However, it requires that the electron system of the quantum dot is not captured in one of the groundstates and remains there, but allows for fluctuations between N and $N+1$, i.e., besides (1.20) at the same time

$$\mu_{\rm S} \geq \mu(N+1;\{V_i\}) \geq \mu_{\rm D} \quad (V_{\rm DS} > 0) \quad \text{or} \quad \mu_{\rm D} \geq \mu(N+1;\{V_i\}) \geq \mu_{\rm S} \quad (V_{\rm DS} < 0) \tag{1.21}$$

has to be fulfilled. Condition (1.20) defines for diverse l and k (l' and k') threshold lines for additional transport channels in the $V_{\rm GS}$ versus $V_{\rm DS}$ plane. Fulfilling this requirement, the transition $|N+1;k\rangle \rightarrow |N;l\rangle$ ($|N;l'\rangle \rightarrow |N+1;k'\rangle$) might be usable for transport at these $\{V_i\}$ if the initial state $|N+1;k\rangle$ ($|N;l'\rangle$) for this transition is reached regularly via other transitions. It leads to the pattern depicted in Fig. 1.9b.

With decreasing the size of a quantum dot, the single-particle eigenenergy spacing $\Delta\varepsilon = \varepsilon_i - \varepsilon_j$ increases and might even exceed the electron charging energy $E_{\rm C}$ due to the electron-electron interaction on the quantum dot: The single-electron charging energy – being a consequence of

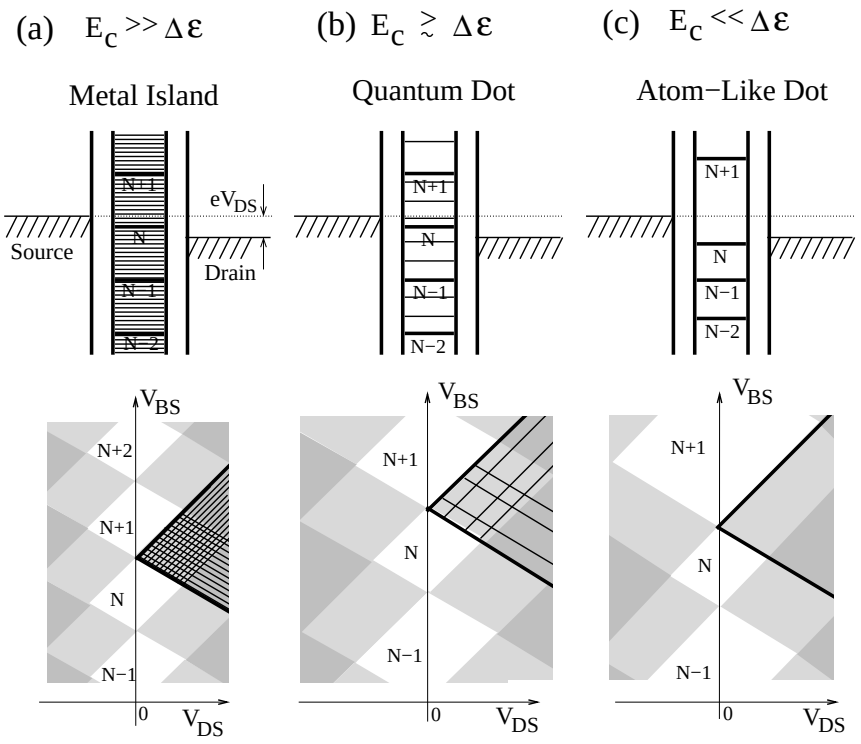

Fig. 1.10: For increasing the ratio $\Delta\varepsilon/E_C$, the energy level scheme shows less transition energies. Therefore less additional transport channels due to (single-particle-)excitations of the quantum dot are expected in the single-electron tunneling regime.

the unscreened electron-electron interaction on the island – scales like $E_C \propto 1/\epsilon D$ with the island diameter D. The level spacing in a parabolic confining potential (taken as the simplest example) scales like $\Delta\varepsilon = \hbar\,\omega_0 = h^2/(2\,m\,D^2)$. As shown in Fig. 1.10, with increasing ratio $\Delta\varepsilon/E_C$, the Coulomb blockade regions in the (V_{GS}, V_{DS}) plane vary more and more in size with the electron number, and a less number of additional channels due to transitions to excited states occur in the single-electron tunneling regime.[3]

In a first approach, the dynamics of electron transport can be described by tunneling rates included in a master equation ansatz. The rate is proportional to the tunneling probability for an electron leading to the transition $|N+1;k\rangle \rightarrow |N;l\rangle$ ($|N;l'\rangle \rightarrow |N+1;k'\rangle$). Obviously such a transition is weighted by the strength of the spatial overlap of the wavefunction of the quantum dot and the respective reservoir. However, such a transition might also obey certain (quasi-)selection rules due to spin conservation or correlation effects of the n-electron system in the quantum dot [27–31]. Therefore, the properties of the $N+1$ and N-electron state are of importance. It might even occur that the occupation of certain excited states blocks the electron transport through the quantum dot [24] – as visible by the negative differential conductance in Fig. 1.7d.

[3]This should be understood as a trend. Indeed, low lying excitations might be possible in a correlated electron system.

1.7 Summarizing the Conditions for Coulomb Blockade

To summarize, the Coulomb blockade effect is observable in electrical transport through small islands if

- the single-electron charging energy exceeds significantly the thermal energy,

$$\frac{\mu(N+1;\{V_i\}) - \mu(N;\{V_i\})}{2} \gg k_{\mathrm{B}}T \qquad (E_{\mathrm{C}} \gg k_{\mathrm{B}}T)\ , \tag{1.22}$$

- the applied drain-source voltage V_{DS} is not too large,

$$e\,|V_{\mathrm{DS}}| < \mu(N+1;\{V_i\}) - \mu(N;\{V_i\}) \qquad (e\,|V_{\mathrm{DS}}| < 2\,E_{\mathrm{C}})\ , \tag{1.23}$$

- the tunnel coupling to the leads is small, i.e., the island can be considered as (quasi-)isolated. Due to Heisenberg's uncertainty relation, the dwell time τ_{H} of an electron on the island has to be so long that the uncertainty $\Delta\varepsilon_{\mathrm{H}} \approx h/\tau_{\mathrm{H}}$ for the energy of an electron on the island does not exceed the single-electron charging energy, i.e.,

$$\tau_{\mathrm{H}} > \frac{2\,h}{\mu(N+1;\{V_i\}) - \mu(N;\{V_i\})} \qquad (\tau_{\mathrm{H}} > h/E_{\mathrm{C}})\ . \tag{1.24}$$

  This is usually achieved if the tunnel barriers to the lead electrodes have a conductance which is much less than $e^2/h \approx (26\,\mathrm{k\Omega})^{-1}$ – the conductance of a ballistic (one-mode) one-dimensional channel.

Since the Coulomb blockade is based on an electrostatic effect, Coulomb blockade and single-electron charging effect can be observed for tunneling through quasi-isolated

- mesoscopic metal islands,
- mesoscopic superconducting islands,
- mesoscopic quantum dots,
- molecules and atom clusters, and
- bounded electron states to impurities.

Several examples will be given in the course of this school.

Depending on the confined electron number, size and effective mass of the electrons, quantum dots resemble in one limit metal-like islands, in the other limit they mimic atom-like properties. Furthermore, the electronic structure of quantum dots can be affected by an applied magnetic field which allows to study the character and degeneracy of electronic states and its influence on electrical transport. Due to their tunability, such quantum dot systems have been used as model systems for investigating interacting N-electron systems and for approaching an understanding of electrical transport through single molecules or single atoms weakly coupled to leads.

1.8 Some Applications of Single-Electron Transistors

1.8.1 SET as a Voltage Signal Amplifier

The single-electron transistor can be used to amplify a voltage signal. Biasing the SET with a constant current I_{DS} as shown in Fig. 1.11, the voltage V_{DS} drops between the source and drain contact which depends in its magnitude on the applied gate voltage V_{GS}. Contour lines of constant current I_{DS} are obtained in the V_{DS} vs. V_{GS} plane parallel to the borderlines defining the different transport regions of the SET as sketched in Fig. 1.4: A change $\mathrm{d}V_{\mathrm{GS}}$ causes due to (1.13) the change

$$\mathrm{d}V_{\mathrm{DS}} = -\frac{C_{\mathrm{G}}}{C_{\mathrm{D}}}\,\mathrm{d}V_{\mathrm{GS}} \qquad \text{or} \qquad \mathrm{d}V_{\mathrm{DS}} = \frac{C_{\mathrm{G}}}{C_{\Sigma} - C_{\mathrm{D}}}\,\mathrm{d}V_{\mathrm{GS}}\ . \tag{1.25}$$

The voltage signal $\mathrm{d}V_{\mathrm{GS}}$ is amplified in $\mathrm{d}V_{\mathrm{DS}}$ if

$$\left|\frac{\mathrm{d}V_{\mathrm{DS}}}{\mathrm{d}V_{\mathrm{GS}}}\right|_{I_{\mathrm{DS}}=\mathrm{const}} > 1\ , \tag{1.26}$$

i.e., *voltage gain* is present. For the SET this can only be obtained for the gate voltage regime where the first relation of (1.25) is valid. That means $C_{\mathrm{G}} > C_{\mathrm{D}}$ [32]. Thus the capacitive coupling of the SET island to the gate electrode where the voltage signal is applied has to be chosen larger than the capacitive coupling to the drain electrode where the output voltage $\mathrm{d}V_{\mathrm{DS}}$ arises. The same can be expressed more general in other words: The SET has to be designed in such a way that the electron charge added to the island induces a larger fraction α_{G} of its image charge on the gate electrode than α_{D} on the drain electrode,

$$\alpha_{\mathrm{G}} > \alpha_{\mathrm{D}} \qquad \text{where} \quad \alpha_{\mathrm{G}} = \frac{C_{\mathrm{G}}}{C_{\Sigma}} \quad \text{and} \quad \alpha_{\mathrm{D}} = \frac{C_{\mathrm{D}}}{C_{\Sigma}} \quad \text{for metal SETs.} \tag{1.27}$$

This is at least required to obtain a voltage gain described by relation (1.26).

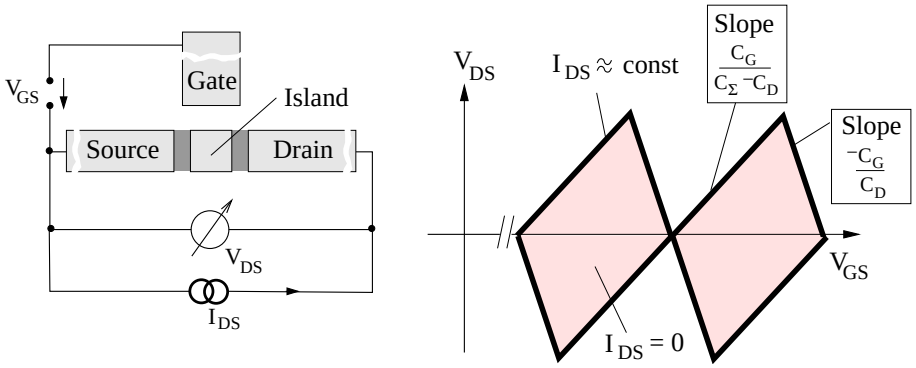

Fig. 1.11: SET as voltage signal amplifier.

1.8.2 SET as an Electrometer Sensitive to a Fraction of the Elementary Charge

The electrostatic potential of electrons on the SET island might not only be changed by voltages applied to adjacent electrodes, but also by putting a charge close to the SET island. As sketched

in Fig. 1.12, adding a negative (positive) charge Q shifts the CBO characteristic towards positive (negative) values of V_{GS}. How sensitive is the single-electron transistor to charges? If the charge $Q = \pm e$ would be added directly to the island, then the CBO characteristic is shifted by one period along the gate voltage axis. In this sense, the SET is a highly sensitive electrometer which is even able to detect easily a fraction of the elementary charge e by the change in its characteristics if the charge is added closely to the island [33]. SETs have been demonstated as electrometers with a charge sensitivity down to $8 \cdot 10^{-8}\, e/\sqrt{\mathrm{Hz}}$ at 10 Hz [34]. Incorporating the SET into a radio-frequency resonance circuit – denoted as *RF-SET* [35] – fast charge fluctuations are detectable ($1.2 \cdot 10^{-5}\, e/\sqrt{\mathrm{Hz}}$ at 1.1 MHz). This high charge sensitivity offers on one hand a *ultrasensitive electrometer*, on the other hand it is a disadvantage for applications where a stable and reproducible SET characteristic is required for a large number of SET devices – like in very-large scale integration (VLSI) of digital circuits. Telegraph noise due to charge fluctuations in the SET surroundings makes them almost useless for this purpose.

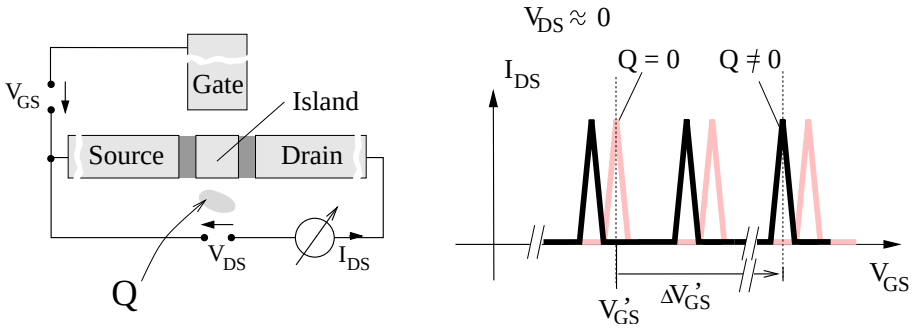

Fig. 1.12: SET as ultrasensitive electrometer.

1.8.3 SET as an Electrostatic Sensor in a Scanning Probe Microscope

The sensitivity of a single-electron transistor to the electrostatic environment can be used to measure chemical potential variations of conducting materials affected by external parameters [36]. A SET can even be incorporated into a scanning probe microscope [37]: As sketched in Fig. 1.13, a SET is fabricated on a microscopic glass tip which is then scanned over a substrate. Monitoring the changes in the SET characteristics as a function of position, the SET can be used as a local probe for the local electrostatic potential variations along the substrate surface. With reducing the distance d between SET and substrate, the capacitance between substrate and SET island reduces roughly like $1/d$. Therefore the CBOs, observed as a function of the voltage applied to the substrate, decrease in their periodicity, squeezing to a fix point on the substrate-SET voltage axis just compensating for the instrinsic contact voltage between SET and substrate. Such an SET on a scanning tip can be considered as an alternative to a scanning force microscope running in the Kelvin probe mode [38] where the local electrostatic force between tip and substrate is minimized by tuning the substrate-tip voltage.

1.8.4 SET as a Current Rectifier

As shown in Fig. 1.4, the capacitance ratios $-C_{\mathrm{D}}/C_{\mathrm{G}}$ and $(C_{\Sigma} - C_{\mathrm{D}})/C_{\mathrm{G}}$ are responsible for the slopes of the boundary lines between Coulomb blockade and single-electron transport regions in

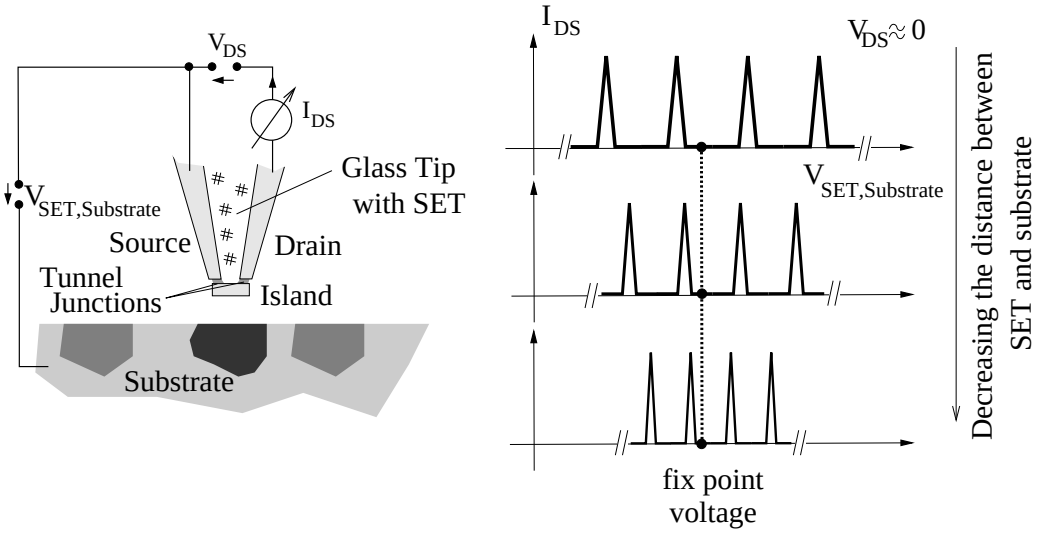

Fig. 1.13: SET as electrostatic sensor on a tip of a scanning probe microscope.

the V_{GS} vs. V_{DS} plane. Therefore, threshold values $V_{\mathrm{DS}}^{(\mathrm{th})}$ at fixed V_{GS} lie usually asymmetrically with respect to $V_{\mathrm{DS}} = 0$. Therefore, SETs display a non-linear $I_{\mathrm{DS}}(V_{\mathrm{DS}})$ characteristics which is tunable by V_{GS}. Due to the non-linearity of such devices around $V_{\mathrm{DS}} = 0$, frequency mixing of ac voltage signals is possible around $V_{\mathrm{DS}} = 0$. Especially a rectification process can occur: An applied ac bias voltage $V_{\mathrm{DS}}(t)$ results in a time-averaged net dc current [39]. Depending on the ratio $C_{\mathrm{D}}/C_{\Sigma}$, three different behaviours are expected (see Fig. 1.14): In the case of $C_{\mathrm{D}}/C_{\Sigma} > \frac{1}{2}$, for a fixed ac bias modulation with $|V_{\mathrm{DS}}(t)| \ll e/C_{\Sigma}$, the sequence in the dc current polarity is zero/positive/negative/zero with increasing V_{GS} from one Coulomb blockade region to the next. In the case $C_{\mathrm{D}}/C_{\Sigma} < \frac{1}{2}$ the sequence is zero/negative/positive/zero. Only in the case $C_{\mathrm{D}}/C_{\Sigma} = \frac{1}{2}$, the net current is basically zero over the whole V_{GS} range.

1.9 The SET for Very-Large Scale Integration (VLSI) of Digital Circuits?

Carrying the current by electrons passing the island one-by-one and being switched on and off by the elementary charge, the single-electron transistor can be considered as the ultimate transistor. Dealing with the smallest amount of charge, it has been suggested with presenting the concept of a SET in the mid 1980´s that integrated circuits based on SETs would lead to lowest power consumption.

It was already pointed out, the sensitivity of a SET on single-electron charge fluctuations is a strong disadvantage in this context [40]. Despite of this, the question arises: Is the SET conceptionally a severe candidate for replacing the MOSFET (Metal-Oxide-Semiconductor Field-Effect Transistor) which is used nowadays as the electronic switch in digital circuits? Both transistor concepts belong to the same class of electrostatically controlled switches and obey therefore the same electrostatic requirements for being a good switch for this application. The answer is basically 'no' [40, 41] which will be further explained in the following.

The overall power dissipation is a severe problem of nowadays microprocessor chips. The only

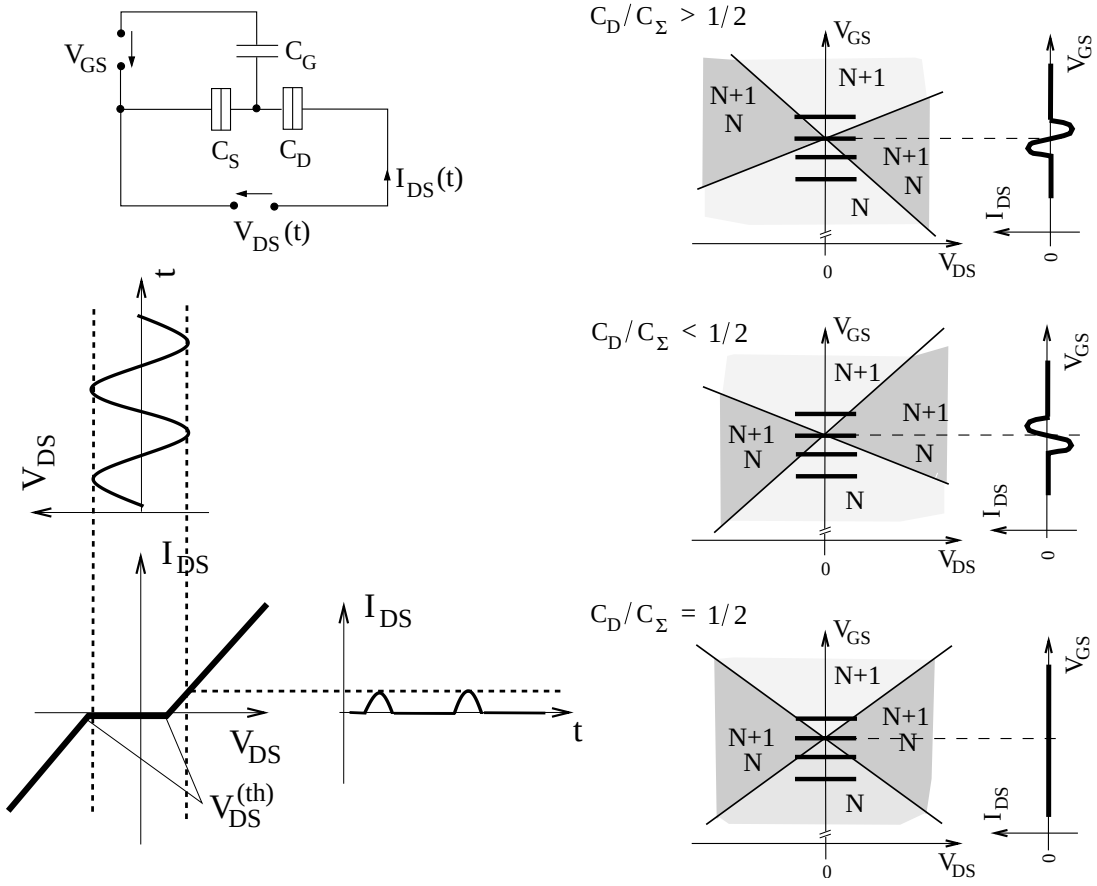

Fig. 1.14: SET as a potential-controlled current rectifier.

known concept for logical circuits, fulfilling the requirement of reliable computation [42] and thereby strongly suppressing the standby power dissipation, is based on two complementary working switches (see Fig. 1.15). It has lead to what is known as CMOS technology. Single-electron transistors can be biased to different working points and then act complementary (one turns on and the other off, controlled by the same voltage signal) [43]. However the circuit concept requires that the transistors have voltage gain. This is hardly to achieve for a single-electron transistor working at room temperature: The island size has to be only few nanometers to reach the high single-electron charging energy, and at the same time the island has to be coupled capacitively stronger to the gate electrode than to the leads ($\alpha_{\mathrm{G}} > \alpha_{\mathrm{D}}$)!

The voltage swing ΔV defines the difference in the voltage levels representing logic '0' and '1'. These are almost given by the positive and negative supply terminals denoted by '0' and 'V_{DD}' in Fig. 1.15. The voltage ΔV drops as the drain-source voltage over the transistor (see Fig. 1.15c and d): The 'on'-current driven through the transistor determines the speed by which the logic gates can switch. The 'off'-current is a leakage causing power dissipation even when the circuit is not doing useful computation (static condition). VLSI requires typically $I_{\mathrm{on}}/I_{\mathrm{off}} > 10^8$ for fulfilling the required performance.

A switch based on tuning an energy barrier electrostatically via a gate voltage leads to the superior characteristic

$$\frac{I_{\mathrm{on}}}{I_{\mathrm{off}}} = \exp \frac{\alpha_{\mathrm{G}}\, e\, \Delta V_{\mathrm{GS}}}{k_{\mathrm{B}} T} \,. \tag{1.28}$$

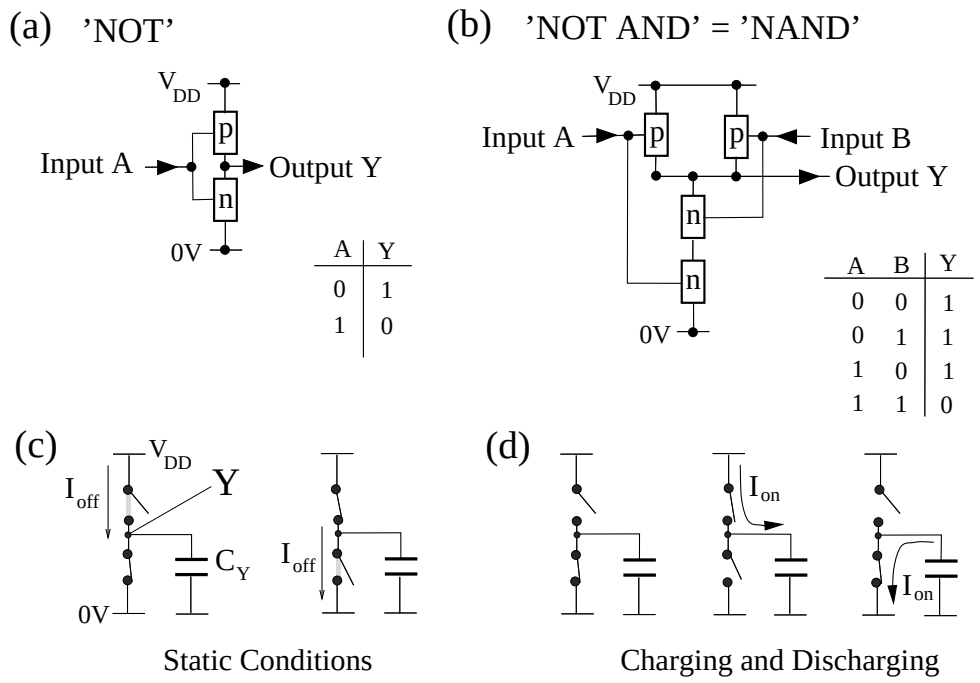

Fig. 1.15: (a), (b) Circuits for logic gates using complementary working switches 'n' and 'p' . (c) To keep the stand-by power dissipation small under static condition, the leakage current $I_{\rm off}$ has to be small. (d) Fast charging and discharging of the output node requires a large $I_{\rm on}$.

The ratio between 'on' and 'off' current depends exponentially on the gate voltage swing $\Delta V_{\rm GS}$ which is at the same time ΔV – the difference between the voltage levels representing the logic '0' and '1' state. The quantity $\alpha_{\rm G}$ is limited by $0 \leq \alpha_{\rm G} \leq 1$ and gives the fraction of image charge which is induced on the controlling gate electrode by a charge in the channel of the electrostatic switch.

MOSFETs offer such an exponential characteristic where $\alpha_{\rm G}$ is close to one. Actually this electrostatic requirement ($\alpha_{\rm G} \to 1$) is mainly the reason why MOSFET have to shrink in *all* spatial dimensions, and therefore the gate oxide of a 0.1 μm MOSFET has been reduced already to 4 nm thickness! For SETs working at room temperature, again, the request on the electrostatics $\alpha_{\rm G}$ close to one is hardly to achieve.

MOSFETs offer for the 'on'-current 0.5 mA per μm channel width – a value which has remained constant over the last decades. Conceptionally, SETs are limited in their capability in driving a current since electrons are passing the island one-by-one. To have a large $I_{\rm on}$, the dwell time of an electron on the island has to be short. Therefore, the tunnel coupling has to be enhanced which leads to a stronger leakage $I_{\rm off}$ in the 'off'-state. The ratio $I_{\rm on}/I_{\rm off}$ cannot follow an exponential dependence on the gate voltage which make SETs worse: For a certain 'on'-current – required for recharging the connections and the inputs of the following logic gates –, the 'off'-current gets too high. This might be compensated by increasing ΔV which again requires that the single-electron charging energy is enlarged, i.e., the island size has to be shrinked even more. We have to state [41]: Single-electron transistor circuits cannot fulfill the expectation of low power dissipation at reasonable speed performance.

Note, these electrostatic constraints are also valid for using molecules as islands as long as their

switching mechanism is purely based on tuning an energy barrier electrostatically. In conclusion, to overcome the severe problems of VLSI, either new circuit design concepts are required – which have not been invented up to now – or a switch has to be found which offers $\alpha_G > 1$. Here is indeed potential for molecules if the switching of the electrical path is controlled by the conformation change of the molecule, induced by an applied electrical field.

1.10 Charge-Stability Diagram of Two-Island Devices

Up to now we have considered only devices with one island embedded between electrodes of defined electrostatic potentials. Examples for two-island arrangements are depicted in Fig. 1.16. Both islands are directly or indirectly connected via tunnel barriers to electrodes. Without a capacitive coupling, the islands do not feel each other. Therefore, in the ideal case, two gate electrode can be used to control independently the charge state of the two islands. As a function of the two gate voltages $V_{G1,S}$ and $V_{G2,S}$, the charge configuration of the two-island arrangement is stable within rectangular regions (indicated by dashed lines in Fig. 1.16). Allowing capacitive interaction between both islands, the gate voltage variations shifts the electrostatic potentials of *both* islands, and the charge states of the islands affect each other. The charge stability diagram divides under such a capacitive coupling between the islands into a *honeycomb pattern* as depicted in Fig. 1.16.

All the two-island arrangements depicted in Fig. 1.16 have this charge stability diagram. Which of these borderlines between the stable regions are actually seen in electrical transport depends on how source and drain electrodes are connected. For the arrangement (I), for instance, only the triple points are visible.

By using quantum dots as islands, molecule-like states can be formed [44, 45] by increasing the tunnel coupling between these 'artifical atoms'. The charge stability diagram pattern deviates

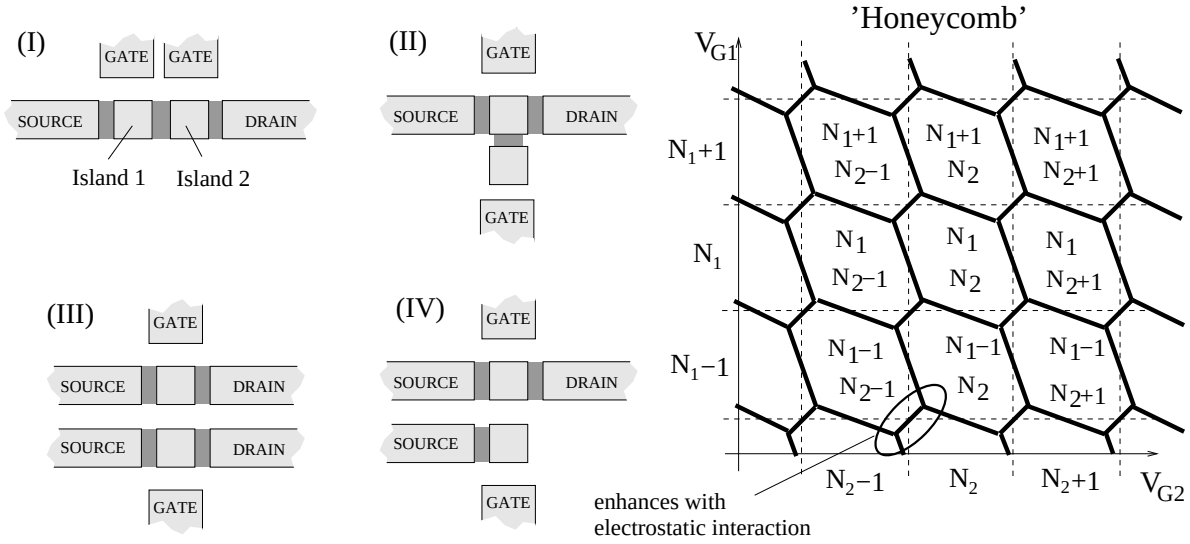

Fig. 1.16: Charge stability diagram valid for the two-island arrangements (I) to (IV) for $V_{DS} = 0$ – denoted as 'honeycomb' pattern.

at the triple points.

1.11 Single-Electron Turnstile and Single-Electron Pump

Having control over single electrons, why not creating a device which transfers a single electron within a cycle – controlled by external ac voltage signals – from source to drain? The current passing such a device is determined by the cycle frequency f,

$$I_{\mathrm{DS}} = e\, f \ . \tag{1.29}$$

Such a devices would allow to define a *current standard* and to close the *quantum metrological triangle* [1, 13] depicted in Fig. 1.17a: Three basic physical quantities – current I, voltage V and frequency f – are linked by three fundamental effects – the Josphson effect connects V with f, the quantum Hall effect V with I, and perhaps a single-electron device obeying (1.29) connects I with f. Closing this triangle would allow to represent their units with higher precision and even to check whether the fundamental relations given in Fig. 1.17 are indeed valid.

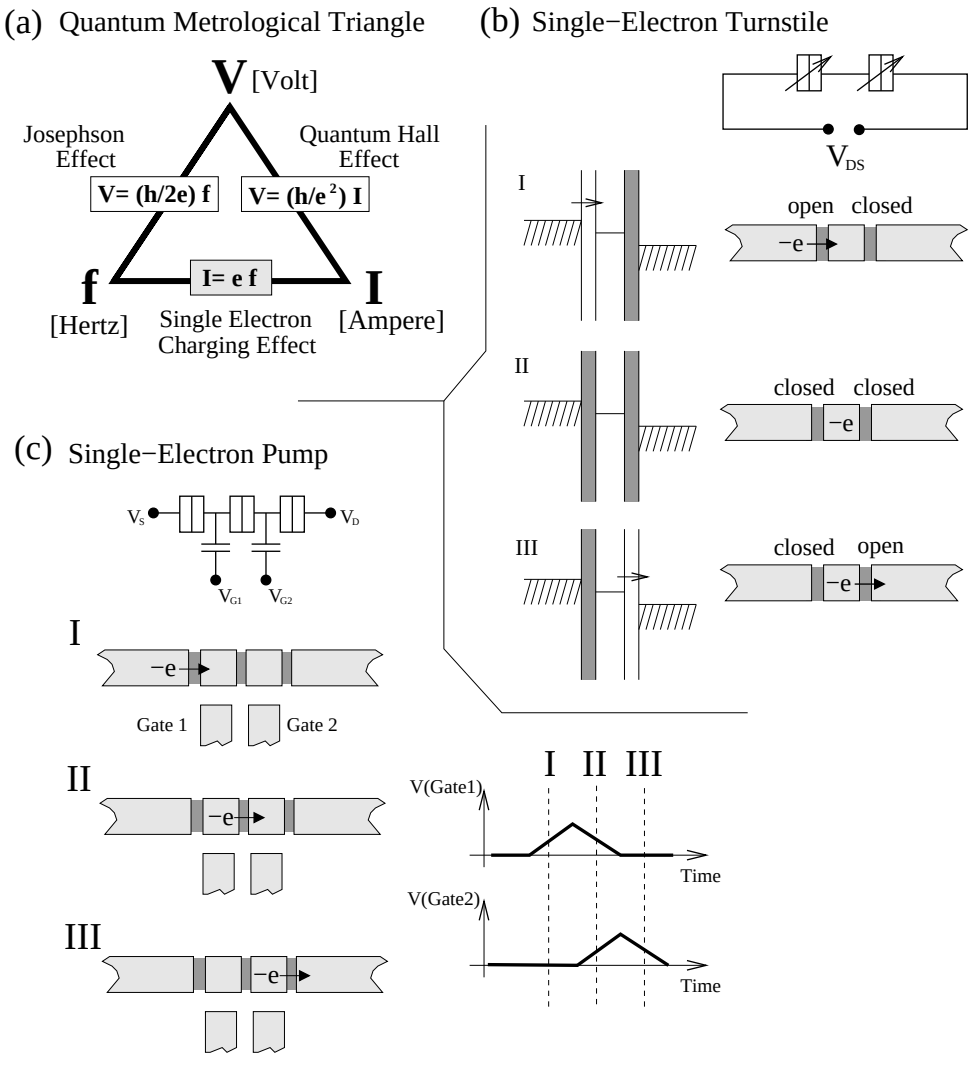

Fig. 1.17: (a) Quantum Metrological Triangle. (b) Single-electron turnstile. (c) Single-electron pump.

One version of such a single-electron device is sketched in Fig. 1.17b denoted as *single-electron turnstile*: The tunnel barriers of a single-electron transistor are tuned similarly to the cycle which the gates of a water lock have to follow to transfer a ship between two water levels through the lock. The Coulomb blockade effect ensures that the island is charged each cycle only with one electron. Such a turnstile with tunable tunnel barriers has been realized by using a split-gate quantum dot [46].

Another version of such a single-electron device obeying (1.29) is shown in Fig. 1.17a: By changing the gate voltages in time in the way sketched in Fig. 1.17c, one electron is transfered within such a cycle via the islands from source and drain. These phase-locked variations of the gate voltages decribe a path which encircles one triple point in the charge stability diagram of Fig. 1.16. The two-terminal arrangement of Fig. 1.17c behaves as a *single-electron pump* [47].

Two islands are enough to perform single-electron pumping. However, several islands in series are required to obtain a high accuracy: Correlated tunneling (co-tunneling) of electrons through the device has to be suppressed because such processes lead to a leakage. Correlated electron tunneling is the topic of section 1.13. An accuracy of $\Delta I_{\rm DS}/I_{\rm DS} \approx 10^{-8}$ has been achieved [48] in single-electron pumps with seven islands in series, i.e., one electron is missed within 10^8 cycles. Unfortunately the current which is driven through a single pump is too small (f about few MHz) for allowing to close the quantum metrological triangle.

Another approach [49, 50] uses surface acoustic waves (SAW) to confine electrons which then have to pass – traveling with this SAW – a small contriction. In another proposal, a certain amount of electrons is shuttled mechanically between source and drain [51].

1.12 Single-Electron Devices as Primary Thermometer

One-dimensional arrays of M small metal islands of almost same size and tunnel junctions offer at low temperature a pronounced nonlinear $I_{\rm DS}(V_{\rm DS})$ characteristic which is rather similar to the one of the single-island arrangement shown in Fig. 1.2. With increasing the temperature to $T > E_{\rm C}/k_{\rm B}$, thermal fluctuations diminish the Coulomb blockade effect and the $I_{\rm DS}(V_{\rm DS})$

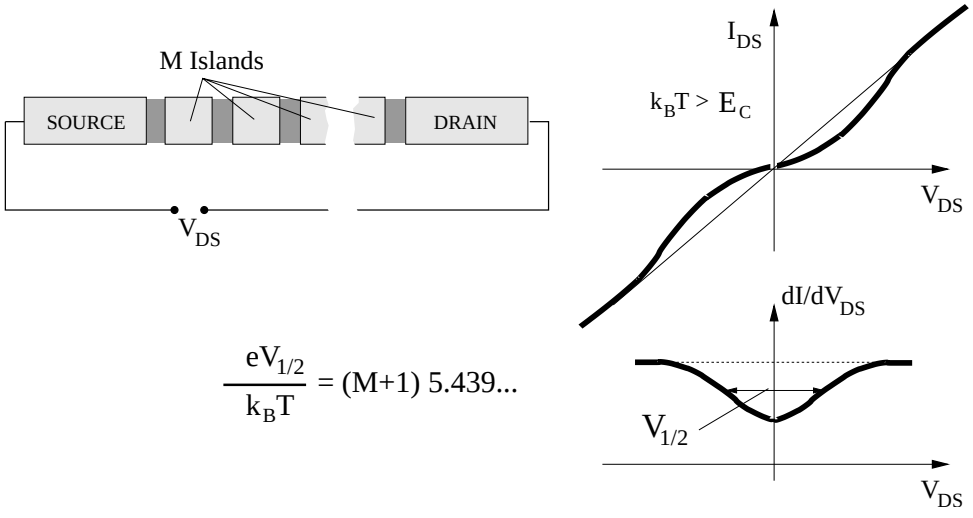

Fig. 1.18: Primary thermometer.

characteristic becomes more and more linear with increasing T. The deviation is still seen close to $V_{\mathrm{DS}} = 0$ which is better resolved by measuring the differential conductance $\mathrm{d}I_{\mathrm{DS}}/\mathrm{d}V_{\mathrm{DS}}$ as a function of V_{DS}: As shown in Fig. 1.18, a dip is visible around $V_{\mathrm{DS}} = 0$. Based on rate equations it can be shown [52, 53] that the depth of the dip scales like $E_{\mathrm{C}}/3k_{\mathrm{B}}T$, whereas the full-width $V_{1/2}$ at half of the dip depth is described by

$$\frac{e\,V_{1/2}}{(M+1)\,k_{\mathrm{B}}T} = 5.439\cdots\ . \tag{1.30}$$

This allows to use such an array as a primary thermometer since $V_{1/2}$ does not depend on the device parameters except of the number M of islands. It has turned out that slight variations in the device parameters (island size and tunnel junction) do not significantly affect the validity of (1.30). Such thermometers are nowadays commercially available products (from Nanoway, Finland). The measurable temperature range depends on the single-electron charging energy E_{C} which can be designed by the junction and island size. Such single-electron devices might be able to replace established temperature standards used at low temperature, i.e., in the range of few milliKelvin to few tens of Kelvin. Two-dimensional arrays of small islands show similar behaviour [53].

1.13 Breakdown of the Single-Electron Tunneling Picture

In the limit of weak tunnel coupling and at low but finite temperature, the dynamics of single-electron transport is usually described by temperature-dependent rate equations [15, 18, 21, 54] revealing the basic features of Coulomb blockade and single-electron tunneling. By this approach, only processes involving a tunneling event of an electron through one of the barriers are taken into account. This does not work in the case of strong tunnel coupling and – as pointed out in Section 1.14 – sometimes even not in the weak tunnel coupling regime.

Besides thermally induced fluctuations in the number of electrons on the island, quantum fluctuations occur and become stronger with increasing the tunnel coupling to the lead electrodes. Simple examples for this are so-called *co-tunneling* events (Fig. 1.19) [55]: An electron from one of the leads occupies the island while at the same time another electron leaves the island to one of the leads. Since the charge state on the island is not changed by this *correlated tunneling* event, no single-electron charging energy has to be paid. Even in the Coulomb blockade regime, this leads to a net current flow between source and drain for $|V_{\mathrm{DS}}| > 0$. The charge state of the island is only virtually changed. Under finite V_{DS} bias, the electron system confined in the quantum dot can even be excited by such correlated tunnel processes (*inelastic cotunneling*). Important to note, transport channels due to correlated tunneling are opened at certain threshold values of V_{DS}, independent of V_{GS} (see Fig. 1.19). This distinguishes them from transport channels opened for single-electron transport. Opening such a cotunneling channel leads to a *step-like* change in the differential conductance $\mathrm{d}I_{\mathrm{DS}}/\mathrm{d}V_{\mathrm{DS}}$ with increasing $|V_{\mathrm{DS}}|$. *Elastic cotunneling*, which uses the transition between the groundstates $|n, 0\rangle$ and $|n+1, 0\rangle$ as the intermediate transition, can already occur at $V_{\mathrm{DS}} = 0$.

This virtual occupation leads effectively to a broadening of the energy levels depicted in the energy schemes for the quantum dot. Usually these correlated tunneling processes can be treated

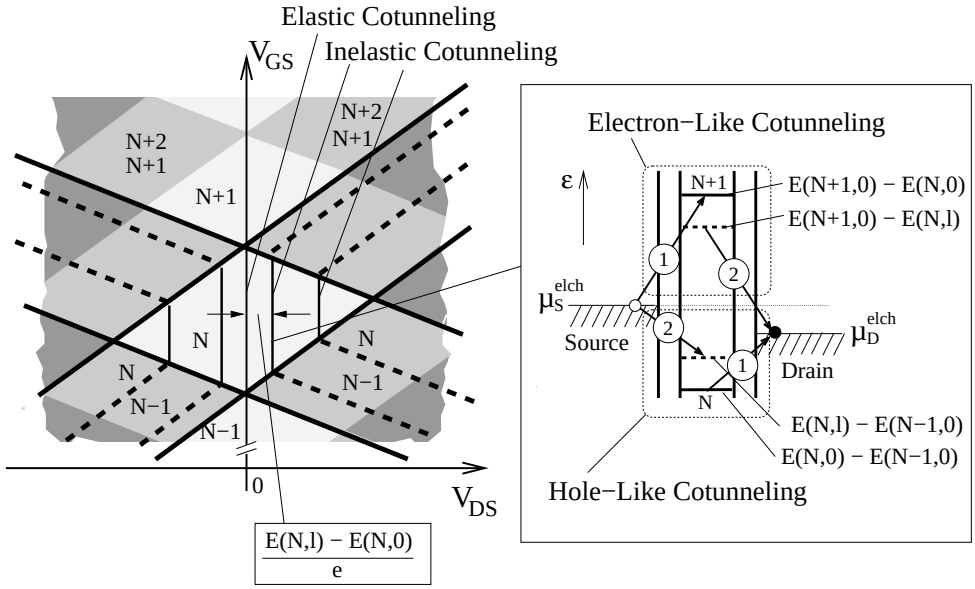

Fig. 1.19: Cotunneling as the simplest correlated tunneling event: Adding an electron while at the same time an electron leaves the island allows electron transport between source and drain even in the Coulomb blockade regime. Transport channels due to cotunneling open at positions in $|V_{DS}| > 0$ (independent of V_{GS}) which are given by the energy difference leading to an excitation of electron system confined in the quantum dot. Such an excitation in the quantum dot can also be taken away by cotunneling.

a small contribution. However, this is not always true as shown in the following.

1.14 Kondo Effect in Single Quantum Dot Systems

Fig. 1.20b shows the differential conductance $\mathrm{d}I_{DS}/\mathrm{d}V_{DS}$ through a small quantum dot (Fig. 1.20a) as a function of V_{DS} and V_{GS}. For the case of weak tunnel coupling to both leads, the Coulomb blockade region is well resolved. With increasing the tunnel coupling while keeping the temperature, the Coulomb blockade region is no longer well defined, but the remarkable feature is the appearance of a peak in the differential conductance at $V_{DS} = 0$ over the whole Coulomb blockade regime [56–59]. It becomes stronger with increasing the tunnel coupling, but disappears with increasing the temperature (Fig. 1.20c). It means that the quantum dot is highly conductive at low temperature and less conductive at high temperature. Important to note, the position of this zero-bias anomaly remains unaffected by V_{GS}, although the electronic states of the dot are shifted by V_{GS}, which indicates that the island is effectively not charged, i.e., that correlated electron tunneling is here of importance. It has been observed [60] that even the conductance $2e^2/h$ is reached for this zero-bias anomaly. Zero-bias anomalies are not observed for all Coulomb blockade regions, i.e., certain requirements have to be fulfilled.

Predicted in 1988 [61, 62] and experimentally demonstrated in 1998 [56], the interpretation of this zero-bias anomaly is based on the so-called Anderson impurity model [63]. The model has been used to describe the Kondo effect observed at low temperature in the resistivity of metal slightly doped with magnetic impurities. The (extended) Anderson impurity model is depicted in Fig. 1.21: A spin-degenerate localized electron state is tunnel coupled to two electron reservoirs. Its energy lies below the Fermi level of the reservoirs, i.e., it is always occupied by an electron

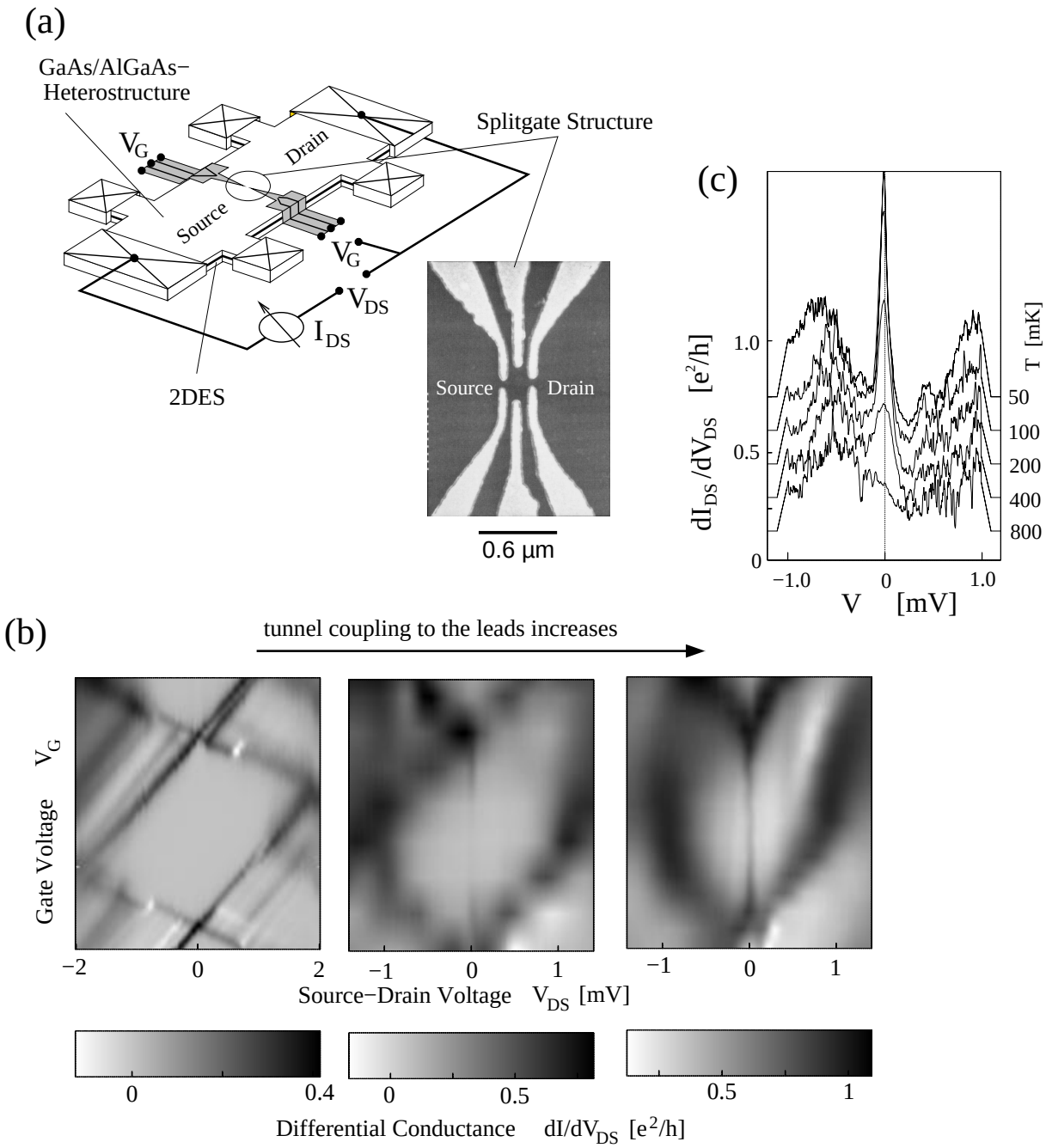

Fig. 1.20: (a) Sketch of the experimental arrangement of a single quantum dot defined in a two-dimensional electron system by electrostatic depletion. (b) Differential conductance as a function of the drain-source voltage and the gate voltage for different tunnel coupling to the leads. A zero-bias anomaly – identified as a Kondo peak – develops at $V_{\rm DS} = 0$ within the Coulomb blockade region. (c) Temperature dependence of the Kondo peak taken in the middle of a Coulomb blockade region (from another sample). (from J. Schmid et al., MPI-FKF)

with spin-up or spin-down. Occupation of the localized state by two electrons at the same time is suppressed due to the electron-electron interaction $U = 2E_{\rm C}$ on the island. Solving this problem, it turns out that correlated electron tunneling of lowest order (cotunneling) is not enough to descibe the transport through such an island: The electronic state of the island hybridizes with the electronic states of the leads forming a spin-singlet state, although the energy level of this

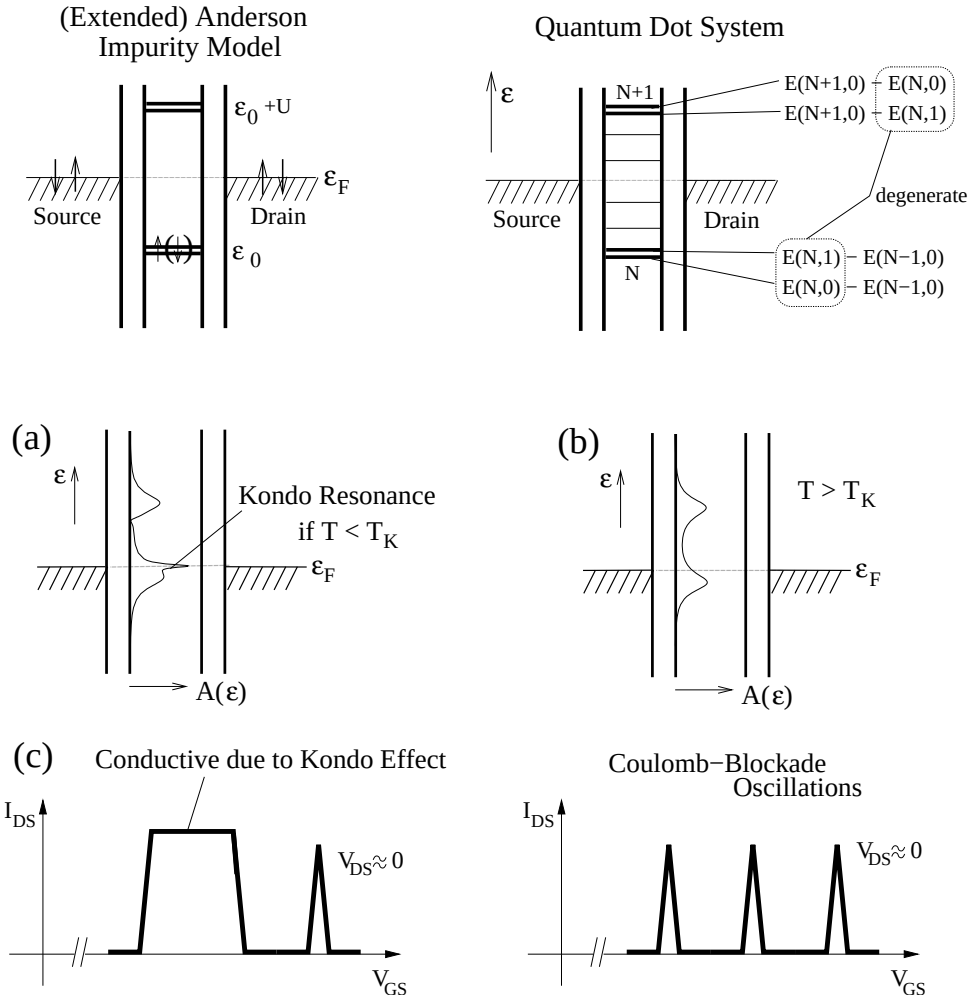

Fig. 1.21: The Anderson impurity model in comparison to the energy scheme of a quantum dot system with (spin-)degenerate groundstate. (a) Solving the model for low temperature, a resonance at the Fermi level is found which disappears at higher temperature (see (b)). (c) At low temperature, the Coulomb blockade disappears in the respective CBO valley but recovers at higher temperature.

localized state is deep below the Fermi level of the reservoirs. At low temperature, even a small tunnel coupling to the leads causes correlated tunneling of electrons permanently flipping the spin state of the island. This leads to an effective density of state on the site of the impurity pinned to the Fermi level of the reservoirs (see Fig. 1.21). Electron transport is possible around $V_{\mathrm{DS}} = 0$. The weaker the tunnel coupling and the deeper the impurity level, the lower the temperature has to be to observe this Kondo effect. The reference scale is given by the so-called *Kondo temperature* T_{K}

$$k_{\mathrm{B}} T_{\mathrm{K}} = \frac{\sqrt{\Gamma U}}{2} \exp\left[-\frac{\pi \left(\varepsilon_{\mathrm{F}} - \varepsilon_0\right) \left(U + \varepsilon_0 - \varepsilon_{\mathrm{F}}\right)}{\Gamma U} \right] \tag{1.31}$$

where the energy Γ describes the broading of the energy level due to the tunnel coupling of the impurity (quantum dot) state to the leads, and $\varepsilon_{\mathrm{F}} - \varepsilon_0$ the energetical distance of the level on the impurity site to the Fermi level of the reservoirs. A large U – basically given by the electron-electron interaction – and large Γ enlarges the Kondo temperature, i.e., the Kondo effect is observed at higher temperature.

Magnetic field dependent measurements reveal that spin-degeneracy usually is responsible for the Kondo effect in quantum dot systems. Suggested by the Constant Interaction Model, at the beginning the Kondo effect has been expected only for an odd number of electron on the quantum dot (*odd-even parity effect*). However, it can also be observed for even electron numbers [59, 64, 65]. The electronic structure of a quantum dot is more complex than assumed by the CIM.

1.15 Two Electrostatically Coupled Single-Electron Transistors: More than the Sum of Two

The Anderson impurity model describes two separate electron systems labeled by an index which is usually identified with the spin quantum number (see Fig. 1.22a). The only interaction between both 'spin' electron systems happens on the impurity (quantum dot) site: Occupation by two electrons at the same time is suppressed due to the Coulomb interaction on this site. Interpreting the 'spin' index of the Anderson impurity model as the index distinguishing between two spatially separated electron systems, another realization of the Anderson impurity model becomes feasible [66]: a system consisting of electrostatically coupled quantum dots with separate leads to each quantum dot (see Fig. 1.22a). The mapping works [66] if (1) an energetical degeneracy is present in occupying either the upper or the lower quantum dot, (2) the groundstate of each quantum dot is not degenerate, excited states are energetically well separated.

An experimental setup to implement this arrangement is shown in Fig. 1.22b: By etching the pattern shown as an SEM image into a GaAs-AlGaAs heterostructure containing two 2DESs separated by a insulating 40 nm thick AlGaAs barrier, two strongly electrostatically coupled quantum dots are formed. By alloying metal contacts and by using top and back gates for locally depleting the upper or lower 2DES, the quantum dots are separately contacted.

In Fig. 1.22c, the conductance through the upper quantum dot is shown as a function of the gate voltages $V_{1,2}$ and V_G (see Fig. 1.22b). A honeycomb-like structure is visible which reflects strong electrostatic interaction between both quantum dots. Along the lines marked by 'a', single-electron tunneling occurs through the upper quantum dot. Along the lines marked by 'c', single-electron fluctuations are possible for the lower quantum dot, but not visible in the current through the upper quantum dot. Along the lines marked by 'b', current through the upper quantum dot is detected – although not expected within the single-electron tunneling picture for electrostatically coupled quantum dots. Along such lines, an energy degeneracy of having an additional electron either on the upper or lower quantum dot exists – one prerequisite of the Anderson model. Due to the predictions for the Anderson model, we expect to see a peak in the differential conductance versus drain-source voltage at the positions along the lines marked by 'b'. Such a trace taken in the middle of a line 'b' is shown in Fig. 1.22d. Th observed peak indicates [67] that a simple co-tunneling process – adding an electron in the upper quantum dot while at the same time taking off an electron from the lower quantum dot (and vice versa) – is not enough to explain the electron transport. Correlated tunneling processes of higher order have to be taken into account – Kondo physics is present.
In conclusion, closely packed single-electron transistors with atom-like islands might show not only electrostatic interaction but might form also a correlated quantum mechanical state mak-

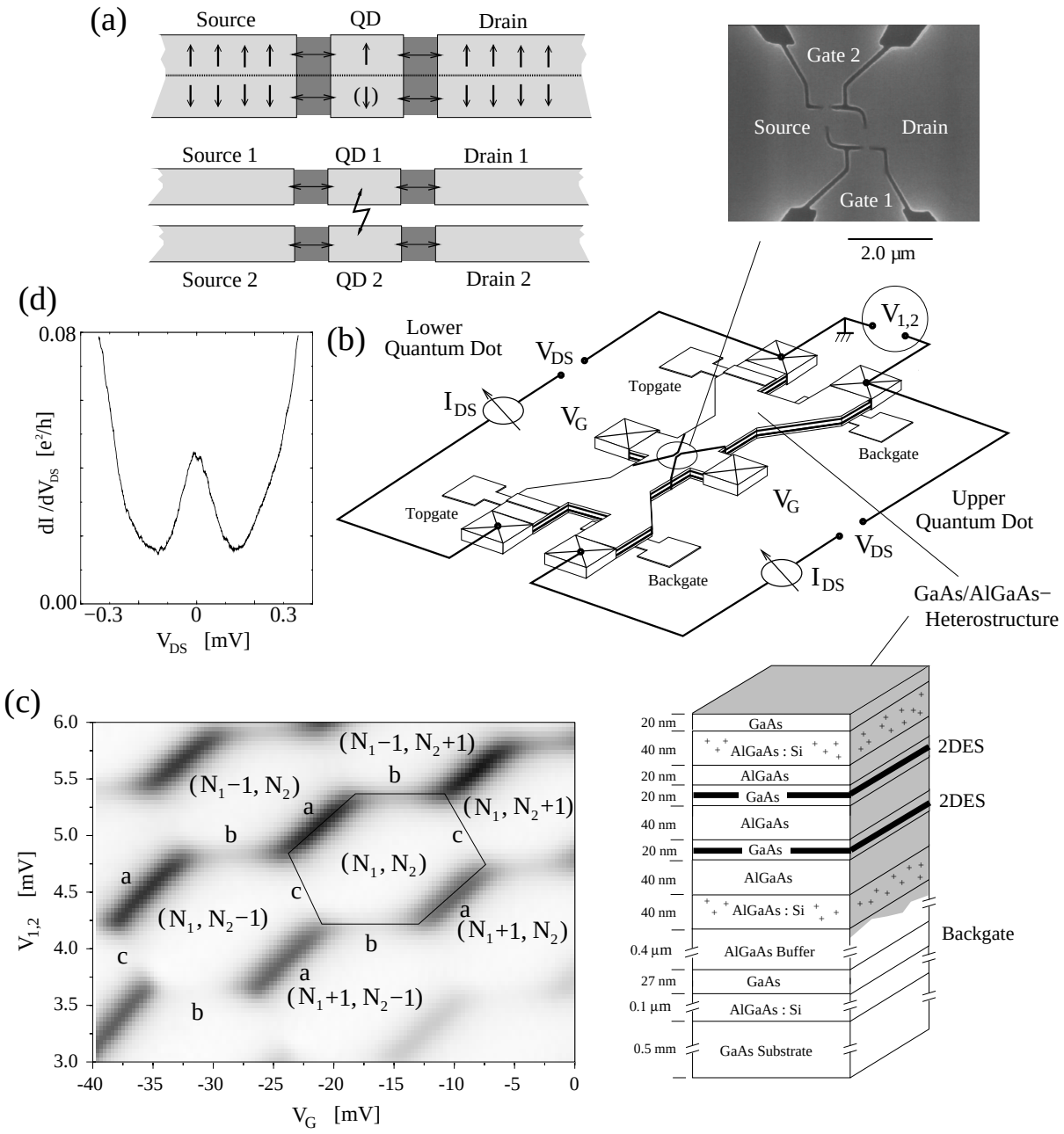

Fig. 1.22: (a) Scheme of the (extended) Anderson impurity model - top: two systems of different spin orientation, bottom: two spatially separated systems. In both cases, the systems interact only electrostatically on the QD site(s). (b) Sketch of the experimental setup of two quantum dots with separate leads. At top, a scanning electron microscope image of the etched pattern defining two quantum dots on top of each other. (c) Conductance through the upper quantum dot versus two gate voltages. (d) Differential conductance versus drain-source voltage taken in the middle of a line marked by 'b' in (c). As expected from the analogy to the Anderson impurity model, a zero-bias anomaly is observed. (from U. Wilhelm et al., MPI-FKF)

ing them highly conductive in the regime where at higher temperature (beyond the Kondo temperature of the arrangement) Coulomb blockade is observed.

References

[1] H. Grabert and M.H. Devoret, editors. *Single Charge Tunneling*, volume B 294 of *NATO ASI Series*. Plenum Press, New York, 1992.

[2] K.K Likharev. Single-electron devices and their applications. *Proceedings of the IEEE*, 87:606, 1999.

[3] U. Meirav and E.B. Foxman. Single-electron phenomena in semiconductors. *Semicond. Sci. Technol.*, 10:255, 1995.

[4] L.P. Kouwenhoven, Ch.M. Marcus, P.L. McEuen, S. Tarucha, R.M Westerwelt, and N.S. Wingreen. Electron transport in quantum dots. In L.L. Sohn and et al., editors, *Mesoscopic Electron Transport*. Kluwer Academic Publishers, 1997.

[5] L.P. Kouwenhoven, D.G. Austing, and S. Tarucha. Few-electron quantum dots. *Rep. Prog. Phys.*, 64:701, 2001.

[6] T. Chakraborty. *Quantum Dots – A survey of the properties of artifical atoms*. North-Holland, Amsterdam, 1999.

[7] G. Schön. Single-electron tunneling. In T. Dittrich, P. Hänggi, G. Ingold, G. Kramer, B. Schön, and W. Zwerger, editors, *Quantum Transport and Dissipation*, chapter 3. VCH, 1997.

[8] H. Schoeller. Transport theory of interacting quantum dots. In L.L. Sohn and et al., editors, *Mesoscopic Electron Transport*. Kluwer Academic Publishers, 1997.

[9] T.M. Eiles, J.M. Martinis, and M.H. Devoret. Even-odd asymmetry of a superconductor revealed by the Coulomb blockade of Andreev reflection. *Phys. Rev. Lett.*, 70:1862, 1993.

[10] M. Tinkham. *Introduction to Superconductivity*. McGraw-Hill, New York, 1996.

[11] E.V. Sukhorukov and D. Loss. Spintronics and spin-based qubits in quantum dots. *phys. stat. sol.*, 224:855, 2001.

[12] Y. Makhlin, G. Schön, and A. Shnirman. Quantum-state engineering with josephson-junction devices. *Rev. Mod. Phys.*, 73:357, 2001.

[13] D.V. Averin and K.K. Likharev. Coulomb blockade of single-electron tunneling, and coherent oscillations in small tunnel junctions. *J. Low Temp. Phys.*, 62:345, 1986.

[14] K.K. Likharev. Single-electron transistors: Electrostatic analogs of the DC SQUIDS. *IEEE Transactions on Magnetics*, 23:1142, 1987.

[15] D.A. Averin, A.N. Korotkov, and K.K. Likharev. Theory of single-electron charging of quantum wells and dots. *Phys. Rev. B*, 44:6199, 1991.

[16] T.A. Fulton and G.D. Dolan. Observation of single-electron charging effects in small tunnel junctions. *Phys. Rev. Lett.*, 59:109, 1987.

[17] L.D. Hallam, J. Weis, and P.A. Maksym. Screening of the electron-electron interaction by gate electrodes in semiconductor quantum dots. *Phys. Rev. B*, 53:1452, 1996.

[18] D. Pfannkuche and S.E. Ulloa. Selection rules for spectroscopy of quantum dots. *Advances in Solid State Physics*, 35:65, 1996.

[19] M. Kastner. Artifical atoms. *Phys. Today*, 46:24, 1993.

[20] R.C. Ashoori. Electrons in artifical atoms. *Nature*, 379:413, 1996.

[21] C.W.J. Beenakker. Theory of Coulomb-blockade oscillations in the conductance of a quantum dot. *Phys. Rev. B*, 44:1646, 1991.

[22] S.M. Reimann and M. Manninen. Electronic structure of quantum dots. *Rev. Mod. Phys.*, 74:1283, 2002.

[23] J. Weis, R.J. Haug, K. v. Klitzing, and K. Ploog. Transport spectroscopy of on a single quantum dot. *Semicond. Sci. Technol.*, 9:1890, 1994.

[24] J. Weis, R.J. Haug, K. v. Klitzing, and K. Ploog. Competing channels in single-electron tunneling through a quantum dot. *Phys. Rev. Lett.*, 71:4019, 1993.

[25] A.T. Johnson, L.P Kouwenhoven, W. de Jong, N.C. van der Vaart, C.J.P.M. Harmans, and C.T. Foxon. Zero-dimensional states and single electron charging in quantum dots. *Phys. Rev. Lett.*, 69:1592, 1992.

[26] E.B. Foxman, P.L. McEuen, N.S. Wingreen, Y. Meir, P.A. Belk, N.R. Belk, and M.A. Kastner. Effects of quantum levels on transport through a Coulomb island. *Phys. Rev. B*, 47:10020, 1993.

[27] J.M. Kinaret, Y. Meir, Wingreen N.S., P. Lee, and X.-G. Wen. Conductance through a quantum dot in the fractional quantum Hall regime. *Phys. Rev. B*, 45:9489, 1992.

[28] D. Weinmann, W. Häusler, and B. Kramer. Spin blockades in linear and nonlinear transport through quantum dots. *Phys. Rev. Lett.*, 74:984, 1995.

[29] J.J. Palacios, L. Martin-Moreno, and C. Tejedor. Magnetotunneling through quantum boxes in a strong-correlation regime. *Europhys. Letters*, 23:495, 1993.

[30] D. Pfannkuche and S.E. Ulloa. Selection rules for transport excitation spectroscopy of few-electron quantum dots. *Phys. Rev. Lett.*, 74:1194, 1995.

[31] K. Jauregui, W. Häusler, D. Weinmann, and B. Kramer. Signatures of electron correlations in the transport properties of quantum dots. *Phys. Rev. B*, 53:1713, 1996.

[32] G. Zimmerli, R.L. Kautz, and J.M. Martinis. Voltage gain in the single-electron transistor. *Appl. Phys. Lett.*, 61:2616, 1992.

[33] P. Lafarge, H. Pothier, E.R. Williams, D. Esteve, C. Urbina, and M.H. Devoret. Direct observation of macroscopic charge quantization. *Z. Phys. B*, 85:327, 1991.

[34] V.A. Krupenin, D.E. Presnov, A.B. Zorin, and M.N. Niemeyer. Aluminum single electron transistors with islands isolated from the substrate. *J. Low Temp. Phys.*, 118:287, 2000.

[35] R.J. Schoelkopf, P. Wahlgren, A.A. Kozhevnikov, P. Delsing, and D.E. Prober. The radio-frequency single-electron transistor (rf-SET): A fast and ultrasensitive electrometer. *Science*, 280:1238, 1998.

[36] Y.Y. Wei, J. Weis, K. von Klitzing, and K. Eberl. Single-electron transistor as an electrometer measuring chemical potential variations. *Appl. Phys. Lett.*, 71:2514, 1997.

[37] M.J. Yoo, T.A. Fulton, H.F. Hess, R.L. Willett, L.N. Dunkelberger, R.J. Chichester, L.N. Pfeiffer, and K.W. West. Scanning single-electron transistor microscopy: Imaging individual charges. *Science*, 276:579, 1997.

[38] M. Nonnenmacher, M.P. O'Boyle, and H.K. Wickramasinghe. Kelvin probe force microscopy. *Appl. Phys. Lett.*, 58:2921, 1991.

[39] J. Weis, R.J. Haug, von K. Klitzing, and K. Ploog. Single-electron tunneling transistor as a current rectifier with potential-controlled current polarity. *Semicond. Sci. Technol.*, 10:877, 1995.

[40] A.N. Korotkov, R.H. Chen, and K.K. Likharev. Possible performance of capacitively coupled single-electron transistors in digital circuits. *J. Appl. Phys.*, 78:2520, 1995.

[41] J. Weis. *Electrical Transport Through Quantum Dot Systms.* Habilitationsschrift, Universität Stuttgart, Germany, 2002.

[42] A.W. Lo. Some thoughts on digital components and circuit techniques. *IRE Trans. on Electronic Computers*, 10:416, 1961.

[43] J.R. Tucker. Complementary digital logic based on the "Coulomb blockade". *J. Appl. Phys.*, 72:4399, 1992.

[44] L. Kouwenhoven. Coupled Quantum Dots as Artifical Molecules. *Sience*, 268:1440, 1995.

[45] R.H. Blick, D. Pfannkuche, R.J. Haug, v. K. Klitzing, and K. Eberl. Formation of a Coherent Mode in a Double Quantum Dot. *Phys. Rev. Lett.*, 80:4032, 1998.

[46] L.P. Kouwenhoven, Johnson A.T., N.C. van der Vaart, A. van den Enden, C.J.P.M. Harmans, and C.T. Foxon. Quantized current in a quantum dot turnstile. *Z. Phys. B*, 85:381, 1991.

[47] H. Pothier, P. Lafarge, C. Urbina, D. Esteve, and M.H. Devoret. Single-Electron Pump Based on Charging Effects. *Europhysics Letters*, 17:249, 1992.

[48] R.L. Kautz, M.W. Keller, and J.M. Martinis. Leakage and counting errors in a seven-junction electron pump. *Phys. Rev. B*, 60:8199, 1999.

[49] V.I. Talyanskii, J.M. Shilton, M. Pepper, C.J.B. Ford, E.H. Linfield, D.A. Ritchie, and G.A.C. Jones. Single-Electron transport in a one-dimensional channel by Radio Frequencies. *Phys. Rev. B*, 56:15180, 1997.

[50] J. Ebbecke, G. Bastian, M. Blöcker, K. Pierz, and F.J. Ahlers. Enhanced quantized current driven by surface acoustic waves. *Appl. Phys. Lett.*, 77:2601, 2000.

[51] A. Erbe, C. Weiss, W. Zwerger, and R.H. Blick. Nanomechanical Resonator Shuttling Single Electrons at Radio Frequencies. *Phys. Rev. Lett.*, 87:096106, 2001.

[52] J.P. Pekola, Hirvi K.P., J.P. Kauppinen, and M.A. Paalanen. Thermometry by arrays of tunnel-junctions. *Phys. Rev. Lett.*, 73:2903, 1994.

[53] J.P. Pekola, L.J. Taskinen, and Sh. Farhangfar. One- and two-dimensional tunnel junction arrays in weak Coulomb blockade regime: Absolute accuracy in thermometry. *Appl. Phys. Lett.*, 76:3747, 2000.

[54] D. Weinmann, W. Häusler, and B. Kramer. Transport properties of quantum dots. *Ann. Physik*, 5:652, 1996.

[55] D.V. Averin and Y.V. Nazarov. Macroscopic quantum tunneling of charge and co-tunneling. In H. Grabert and M.H. Devoret, editors, *Single Charge Tunneling*, volume B 294 of *NATO ASI Series*, pages 217–247. Plenum Press, New York, 1992.

[56] D. Goldhaber-Gordon, H. Shtrikman, D. Mahalu, D. Abusch-Magder, U. Meirav, and M.A. Kastner. Kondo effect in a single-electron transistor. *Nature*, 391:156, 1998.

[57] S.M. Cronenwett, T.H. Oosterkamp, and L.P. Kouwenhoven. A tunable Kondo effect in quantum dots. *Science*, 281:540, 1998.

[58] J. Schmid, J. Weis, K. Eberl, and K. v. Klitzing. A quantum dot in the limit of strong coupling to reservoirs. *Physica B*, 256:182, 1998.

[59] J. Schmid, J. Weis, K. Eberl, and K. v. Klitzing. Absence of odd-even parity behaviour for Kondo resonances in quantum dots. *Phys. Rev. Lett.*, 84:5824, 2000.

[60] W.G. van der Wiel, S. De Franceschi, T. Fujisawa, J.M. Elzerman, S. Tarucha, and L.P. Kouwenhoven. The Kondo effect in the unitary limit. *Science*, 289:210, 2000.

[61] L.I. Glazman and M.É. Raĭkh. Resonant Kondo transparency of a barrier with quasilocal impurity states. *JETP Lett.*, 47:453, 1988.

[62] T.K. Ng and P.A. Lee. On-site Coulomb repulsion and resonant tunneling. *Phys. Rev. Lett.*, 61:1768, 1988.

[63] P.W. Anderson. Localized magnetic states in metals. *Phys. Rev.*, 124:41, 1961.

[64] S. Sasaki, S. De Franceschi, J.M. Elzerman, W.G. van der Wiel, M. Eto, S. Tarucha, and L.P. Kouwenhoven. Kondo effect in an integer-spin quantum dot. *Nature*, 405:764, 2000.

[65] M. Keller, U. Wilhelm, J. Schmid, J. Weis, K. v. Klitzing, and K. Eberl. Quantum dot in high magnetic fields: Correlated tunneling of electrons probes the spin configuration at the edge of the dot. *Phys. Rev. B*, 64:033302, 2001.

[66] U. Wilhelm, J. Schmid, J. Weis, and K. v. Klitzing. Two electrostatically coupled quantum dots as a realization of the Anderson impurity model. *Physica E*, 9:625, 2001.

[67] U. Wilhelm, J. Schmid, J. Weis, and K. v. Klitzing. Experimental evidence for spinless Kondo effect in two electrostatically coupled quantum dot systems. *Physica E*, 14:385, 2002.